

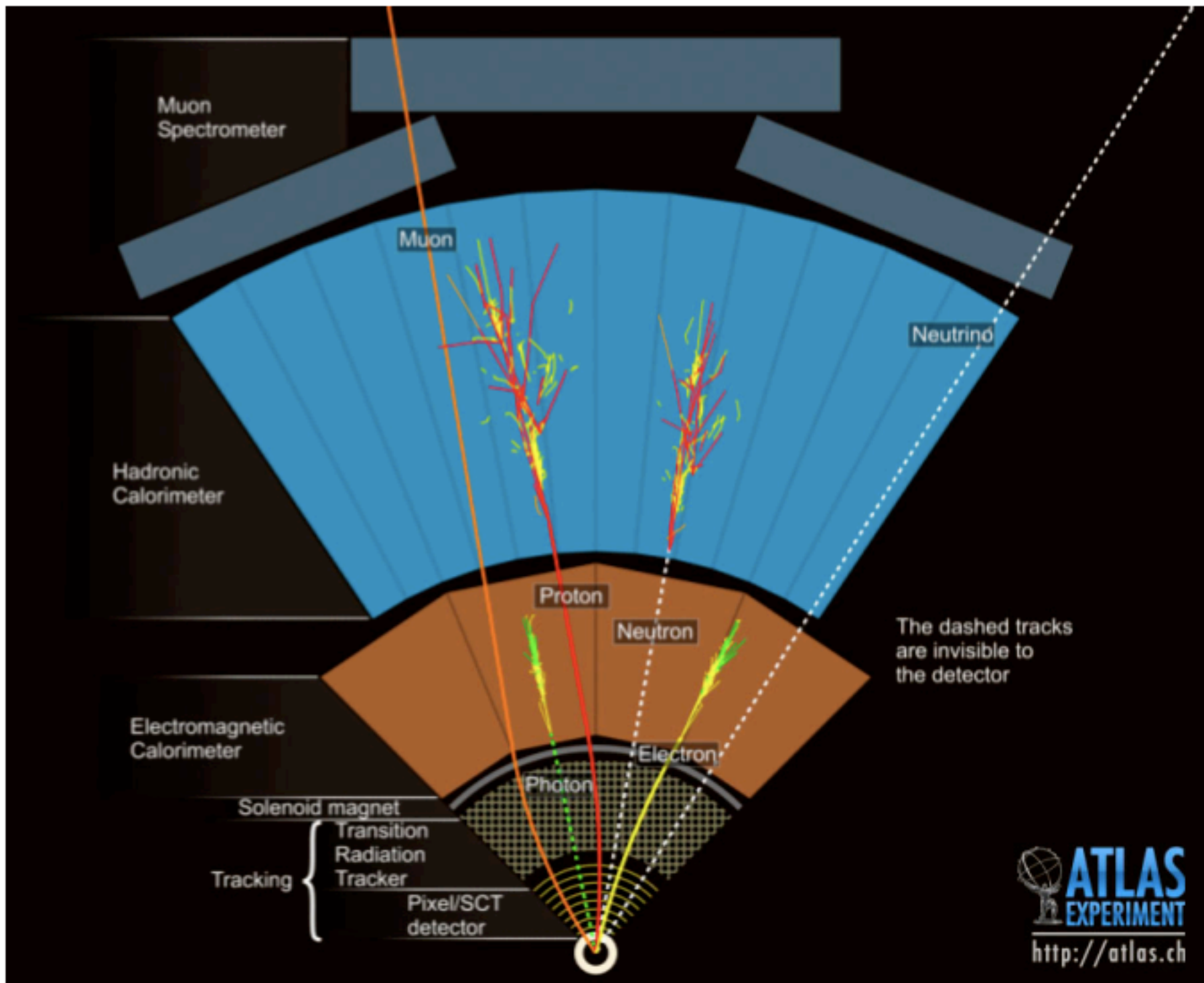
An aerial photograph of a rural landscape with a large white circle overlaid on it. The landscape consists of a patchwork of green and brown fields, with some buildings and roads scattered throughout. The sky is a clear, deep blue. The text is overlaid on the image in white and yellow colors.

Experimentele Technieken

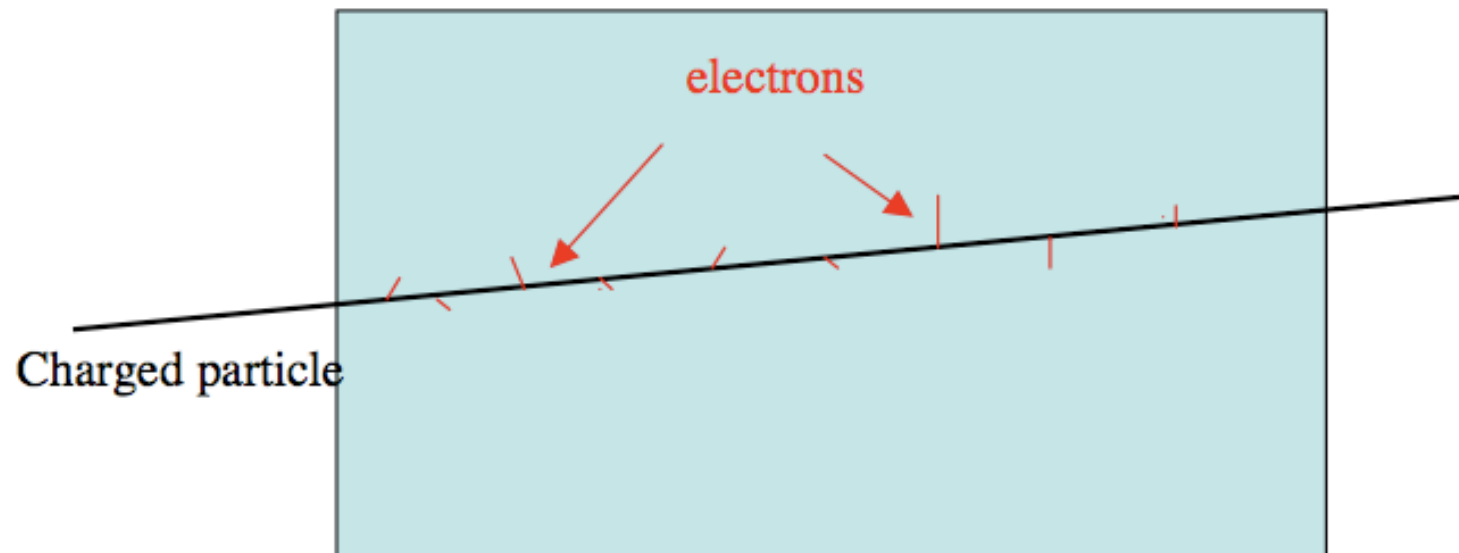
*in de Hoge Energie Fysica
en verdere toepassingen*

Deel 3: Spoor detectoren

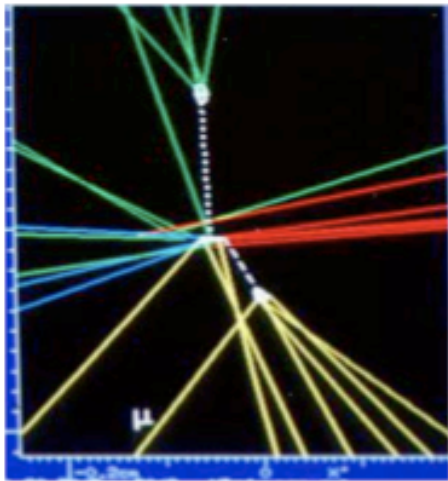
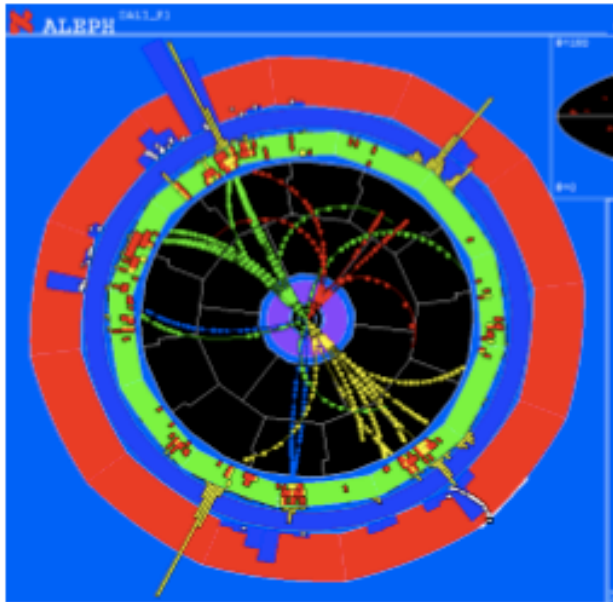
Prof. Dr. Albert De Roeck
CERN, Geneva, Switzerland
Universiteit Antwerpen
UC-Davis, California, US



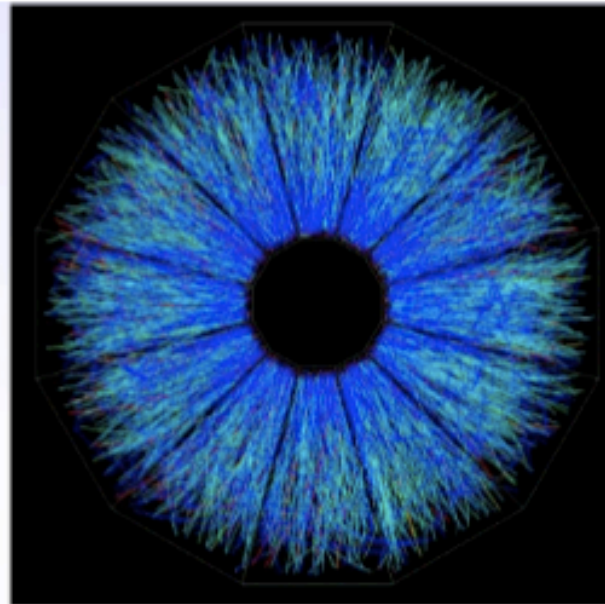
Interactions with Matter



**e+ e- collision in the
ALEPH Experiment/LEP.**

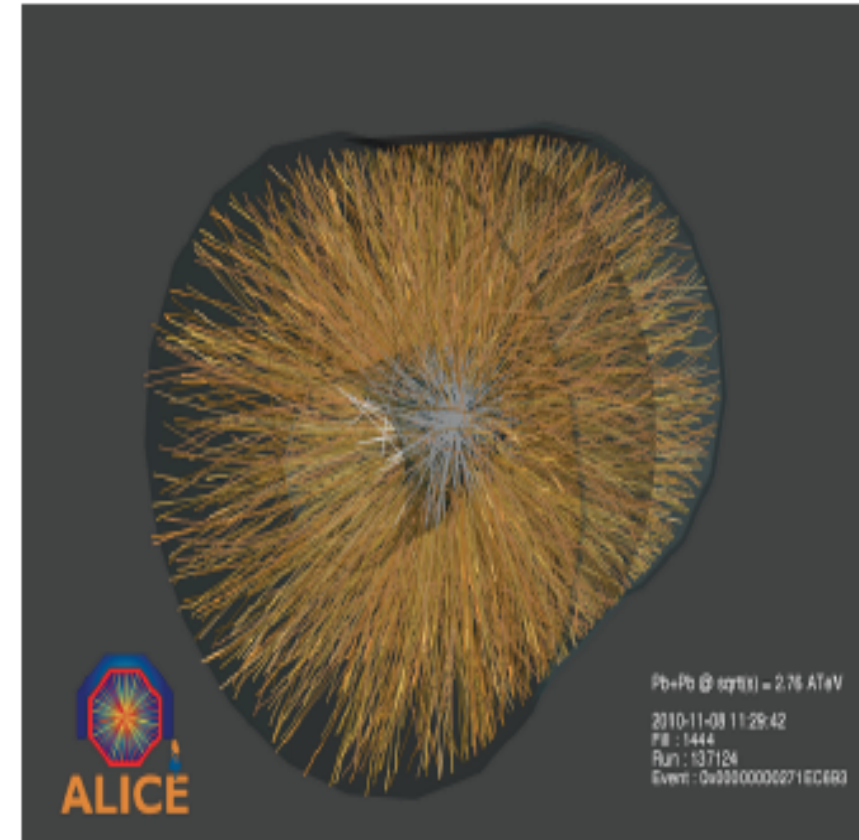


**Au+ Au+ collision in the
STAR Experiment/RHIC
Up to 2000 tracks**



**Pb+ Pb+ Kollision in the ALICE
Experiment/LHC**

Up to 40 000 tracks/collision



Multiple Scattering

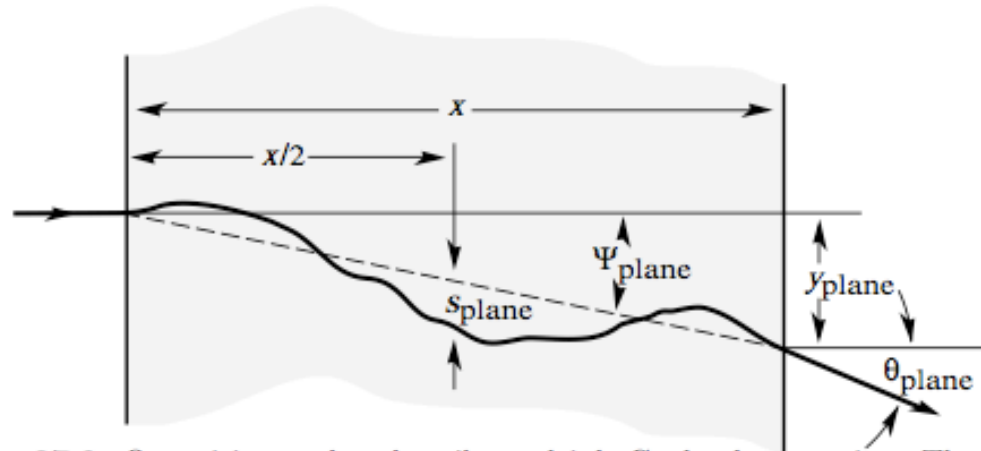


Figure 27.9: Quantities used to describe multiple Coulomb scattering. The particle is incident in the plane of the figure.

$$\begin{aligned}\psi_{\text{plane}}^{\text{rms}} &= \frac{1}{\sqrt{3}} \theta_{\text{plane}}^{\text{rms}} = \frac{1}{\sqrt{3}} \theta_0, \\ y_{\text{plane}}^{\text{rms}} &= \frac{1}{\sqrt{3}} x \theta_{\text{plane}}^{\text{rms}} = \frac{1}{\sqrt{3}} x \theta_0, \\ s_{\text{plane}}^{\text{rms}} &= \frac{1}{4\sqrt{3}} x \theta_{\text{plane}}^{\text{rms}} = \frac{1}{4\sqrt{3}} x \theta_0.\end{aligned}$$

A particle which traverses a medium is deflected by small angle **Coulomb scattering** from nuclei. For hadronic particles also the strong interaction contributes.

The **angular deflection** after traversing a distance x is described by the **Molière theory**. The angle has roughly a **Gauss distribution**, but with larger tails due to Coulomb scattering.

Defining: $\theta_0 = \theta_{\text{plane}}^{\text{rms}} = \frac{1}{\sqrt{2}} \theta_{\text{space}}^{\text{rms}}$

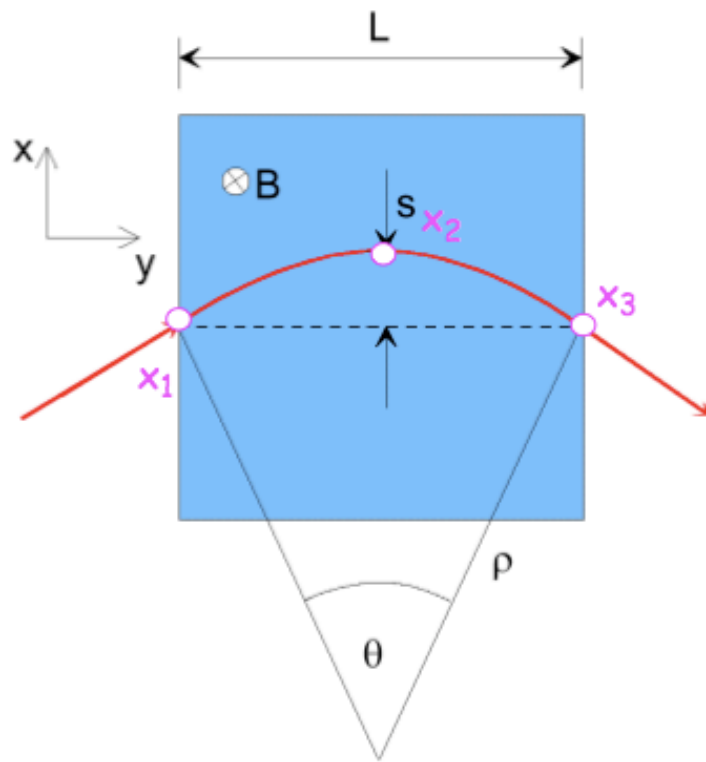
Gaussian approximation:

$$\theta_0 = \frac{13.6 \text{ MeV}}{\beta c p} z \sqrt{x/X_0} \left[1 + 0.038 \ln(x/X_0) \right]$$

x/X_0 is the thickness of the material in radiation length.

Momentum Measurements in B-field

The momentum is measured from the **sagitta** s , which gives the **curvature** ρ of the track in the magnetic field.

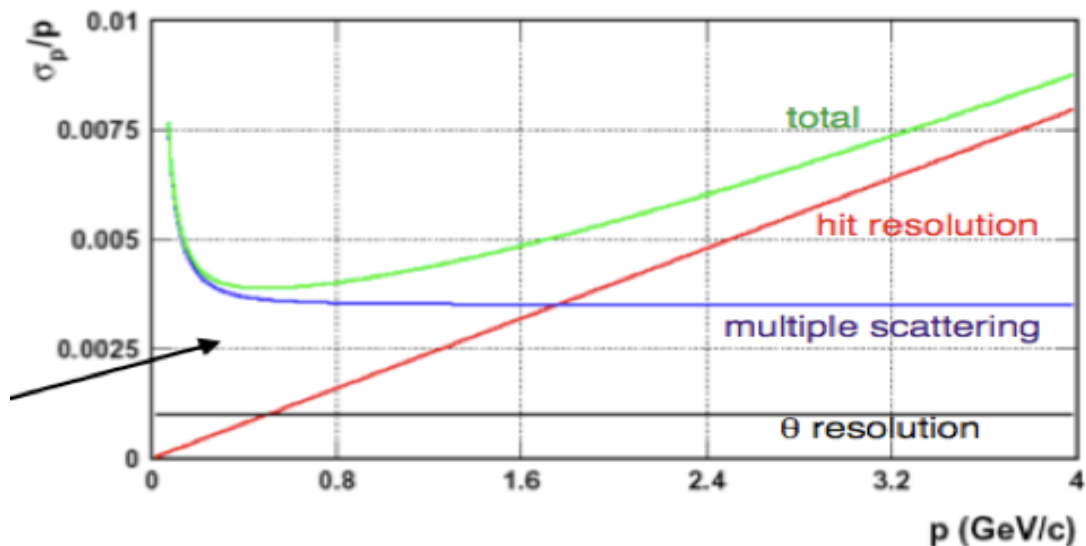


Examples

Transverse momentum: $p_T = qB\rho$
 $p_T[\text{GeV}] = 0.3 B[\text{T}] \rho[\text{m}]$

$$\frac{L/2}{\rho} = \sin \frac{\theta}{2} \approx \frac{\theta}{2} \quad (\text{for small } \theta) \Rightarrow \theta \approx \frac{L}{\rho} = \frac{0.3BL}{p_T}$$

$$s = \rho \left(1 - \cos \frac{\theta}{2}\right) \approx \rho \left(1 - \left(1 - \frac{1}{2} \frac{\theta^2}{4}\right)\right) = \rho \frac{\theta^2}{8} \approx \frac{0.3BL^2}{8p_T}$$

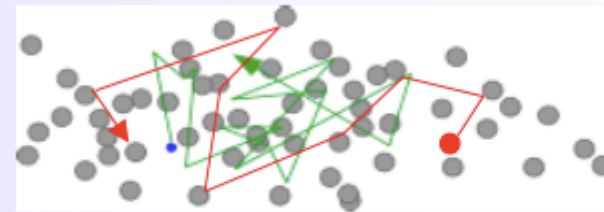


Drift and Diffusion in Gases

from L.Ropelewski

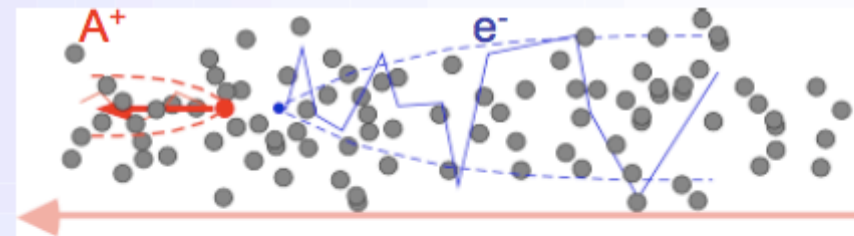
$E=0$ thermal diffusion

$$\langle \mathbf{v} \rangle_t = 0$$



$E>0$ charge transport and diffusion

$$\langle \mathbf{v} \rangle_t = \mathbf{v}_D$$



Electric Field

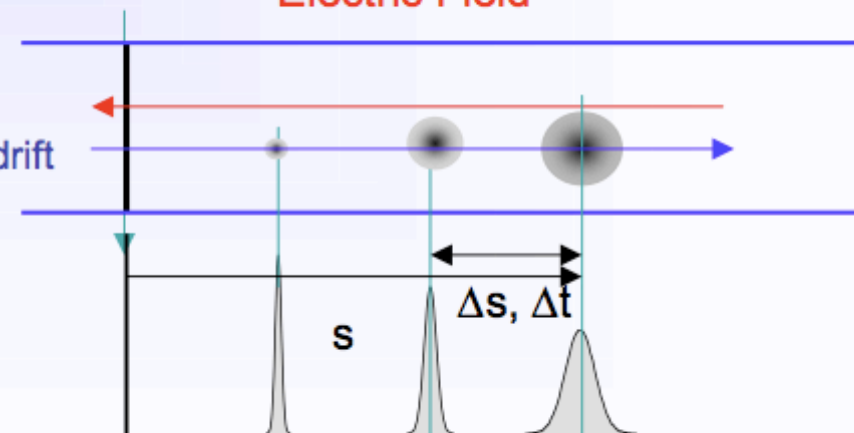
$$v_D = \frac{\Delta s}{\Delta t}$$

$$\sigma_x = \sqrt{2Dt} = \sqrt{2D \frac{s}{v_D}}$$

Electron swarm drift

Drift velocity

Diffusion



Lorentz Angle in a magnetic Field

Lorentz angle (deflection angle of drift electrons due to magnetic field)

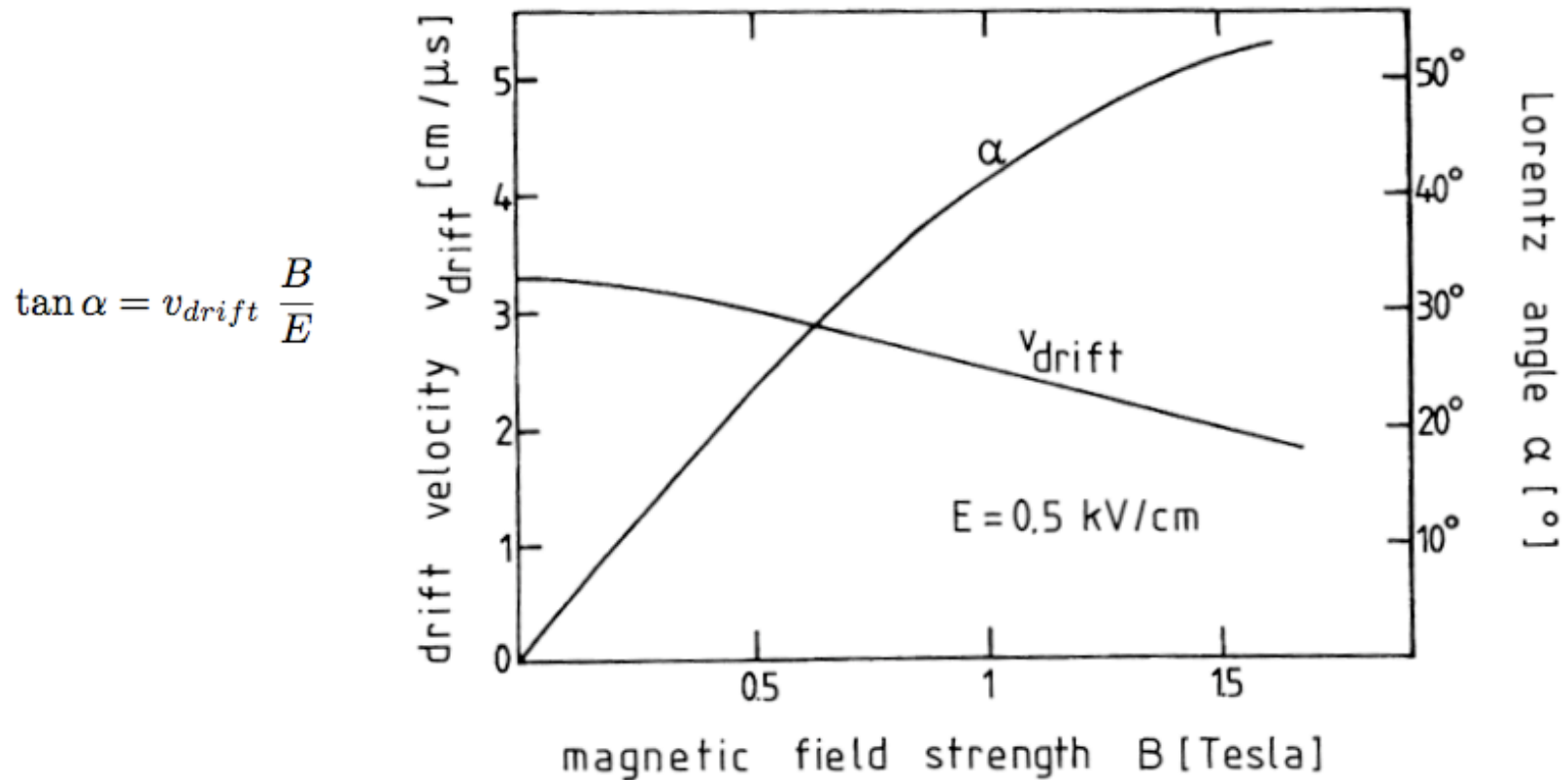


Fig. 1.21. Dependence of the electron drift velocity \vec{v}_{drift} and the Lorentz angle α on the magnetic field for low electric field strengths (500 V/cm) in a gas mixture of argon (67.2%), isobutane (30.3%) and methylal (2.5%) [51, 95].

History of Tracking: Cloud Chambers

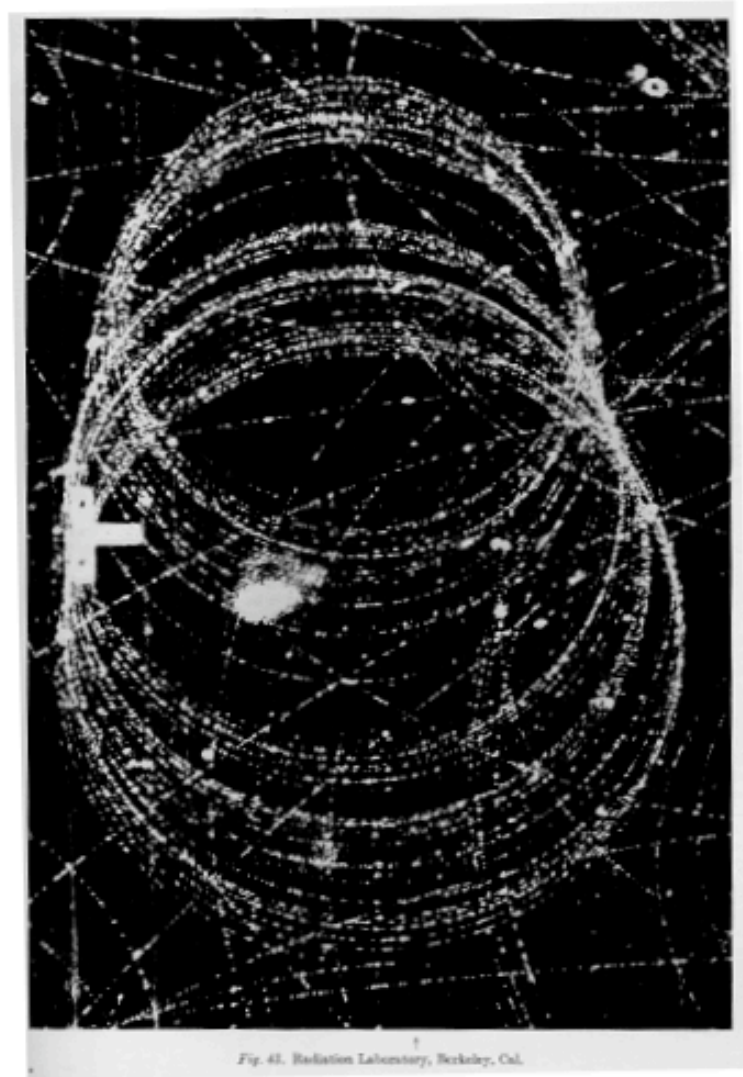


Fig. 41. Radiation Laboratory, Berkeley, Cal.

Fast electron in a magnetic field at the Bevatron, 1940

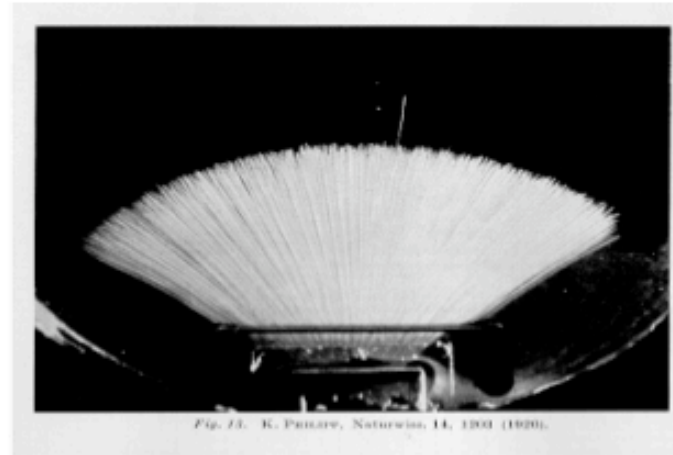


Fig. 21. K. Prineas, Nature, 114, 1001 (1920).

α -particles
in air.

In cloud chambers a charged particle causes condensation of a supersaturated gas.

The picture (left) shows an electron with 16.9 MeV initial energy.

It spirals about 36 times in the magnetic field.

Nobel prizes related to cloud chamber development:

C. T. R. Wilson, 1927

P.M.S. Blackett, 1948 (triggered chambers)

History of Tracking: Cloud Chambers

CERN Courier

Sep 27, 2012

From the October 1969 issue

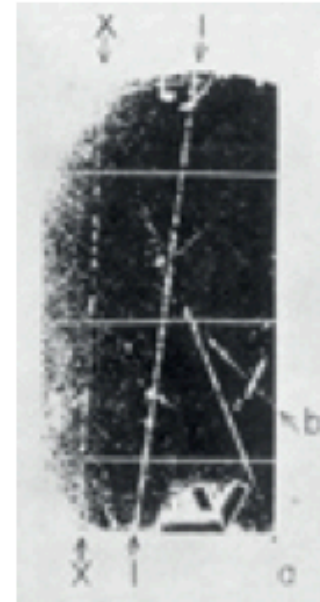
Quark candidates in Sydney

A report, by a team from the Cornell-Sydney University Astronomy Centre, Australia, on a high-energy cosmic-ray search which seems to have evidence for quarks, appeared in *Physical Review Letters* on 22 September. A preliminary announcement was made at the 11th

International Conference on Cosmic Ray

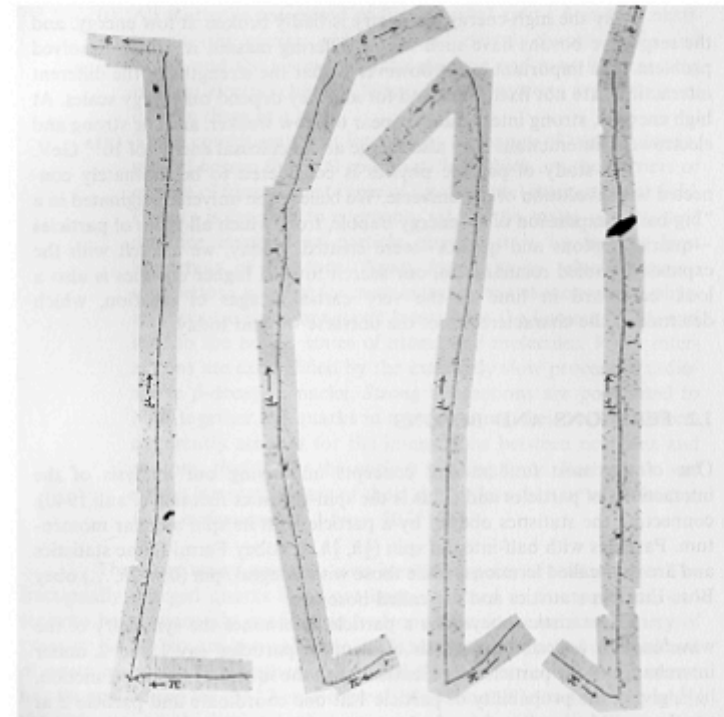
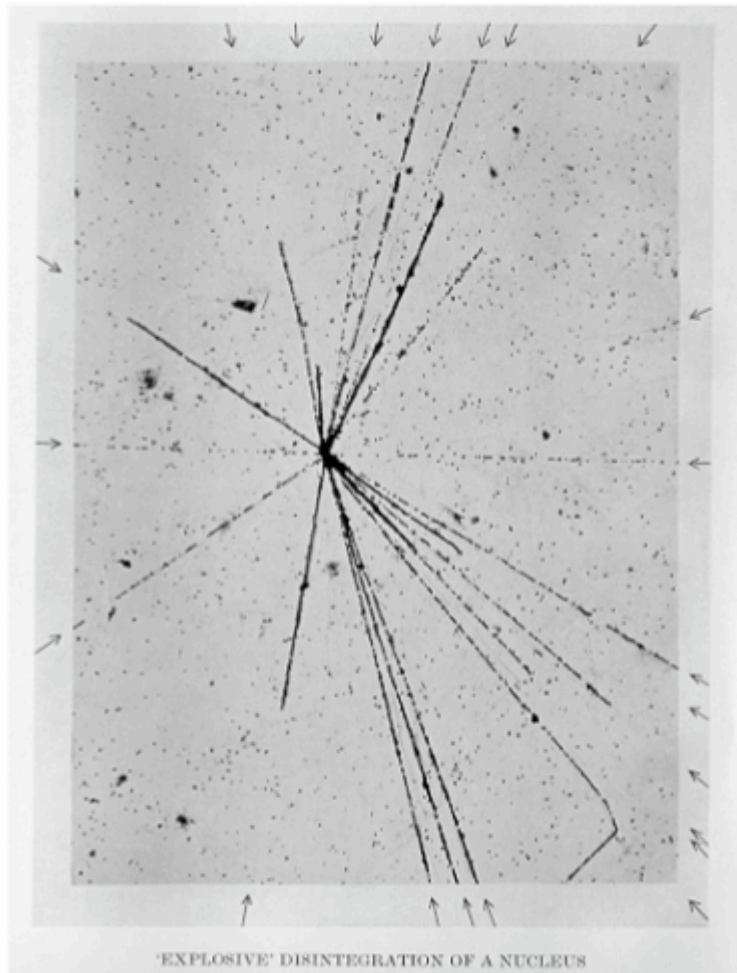
Physics in Budapest, 25 August to 4 September, and on 8 September L S Peak, who participated

in the experiment with L Cairns, R L S Woolcott and team leader C B A McCusker, spoke at CERN about their intriguing findings.



Wilson cloud chamber

History of Tracking: Emulsion



Discovery of muon and pion

Emulsion detectors are still used today: Opera experiment at Gran Sasso for the identification of tau decays.

History of Tracking: Bubble Chambers

Cloud chamber: supersaturating a gas with a vapor.

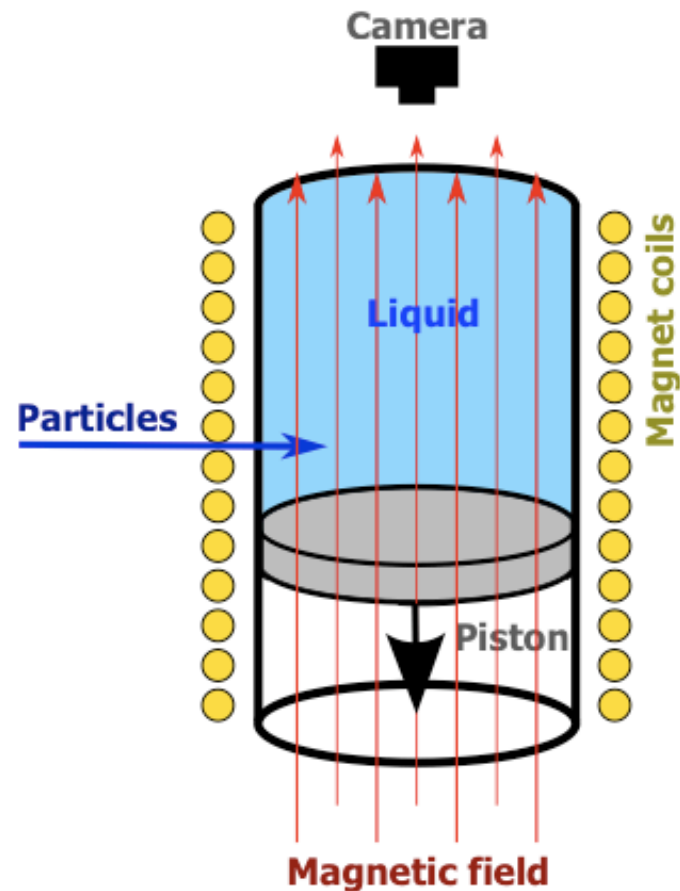
Bubble chamber: superheated liquid. Invented by Donald A. Glazer, Nobel Prize 1960.

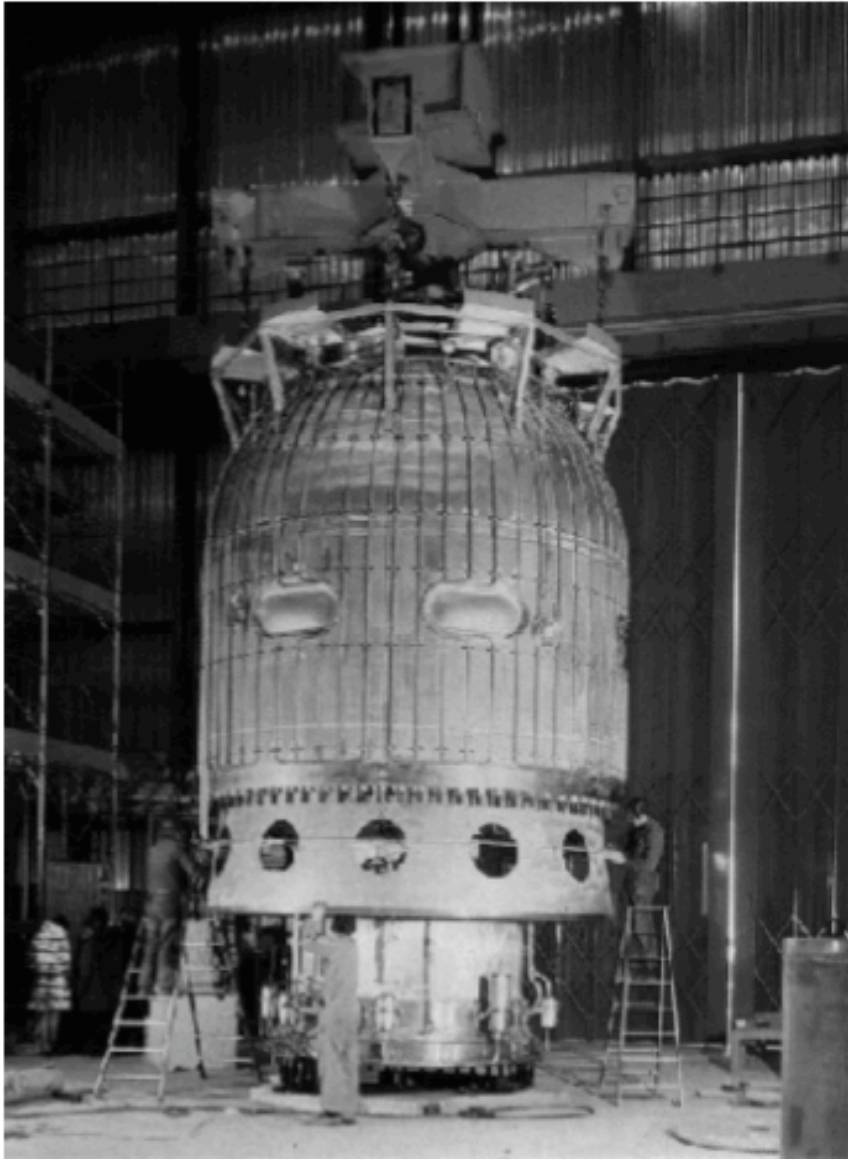
A particle depositing energy along it's path makes the liquid boil and forms bubbles.



The 80-inch Bubble Chamber

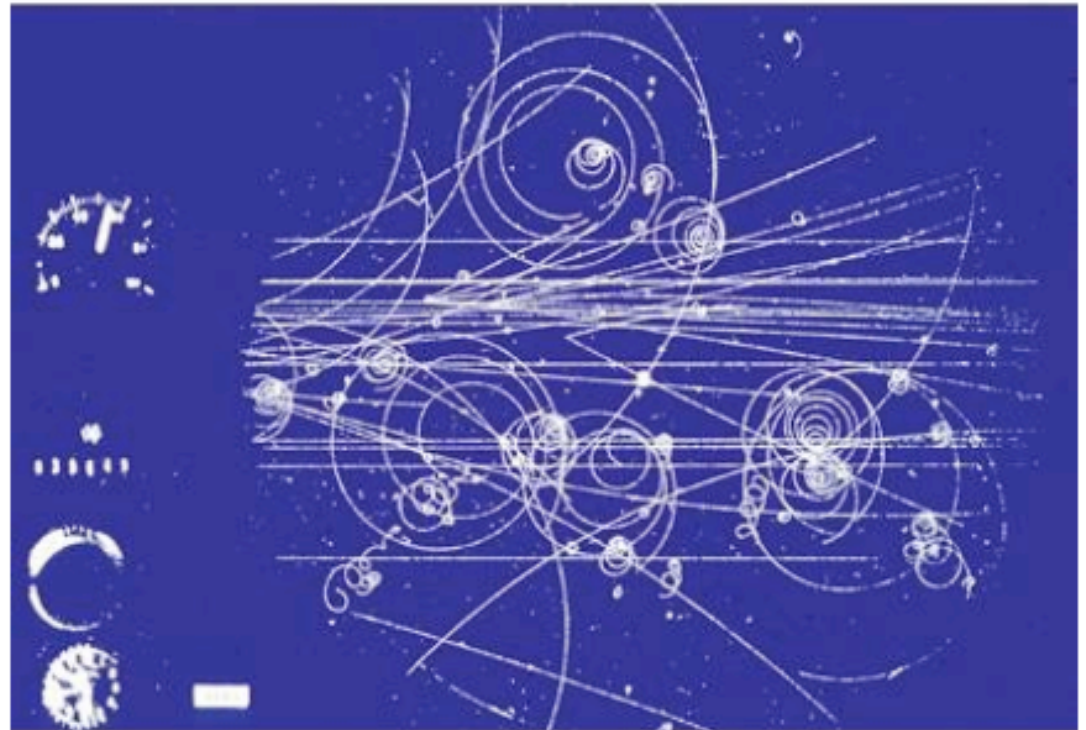
BNL, First Pictures 1963, 0.03s cycle





3.7 meter hydrogen bubble chamber at CERN, equipped with the largest superconducting magnet in the world at that time.

During its working life from 1973 to 1984, the "Big European Bubble Chamber" (BEBC) took over 6 million photographs.



Can be seen outside the Microcosm Exhibition

Bubble Chambers

The excellent position ($5\mu\text{m}$) resolution and the fact that target and detecting volume are the same (H chambers) makes the Bubble chamber almost unbeatable for reconstruction of complex decay modes.

The drawback of the bubble chamber is the low rate capability (a few tens/ second). E.g. LHC 10^9 collisions/s.

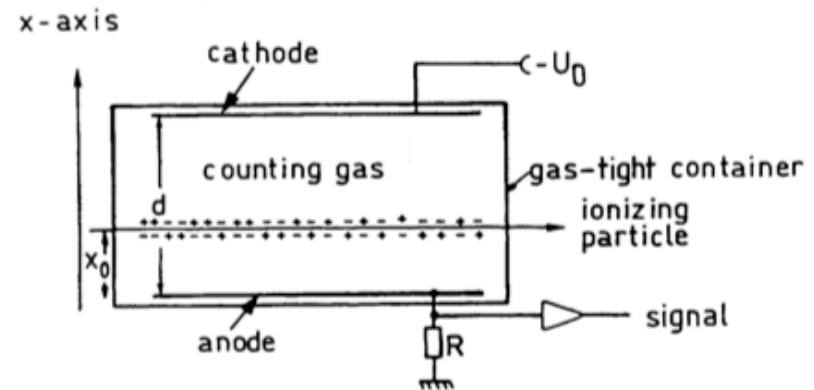
The fact that it cannot be triggered selectively means that every interaction must be photographed.

Analyzing the millions of images by 'operators' was a quite laborious task.

That's why electronics detectors took over in the 70ties.

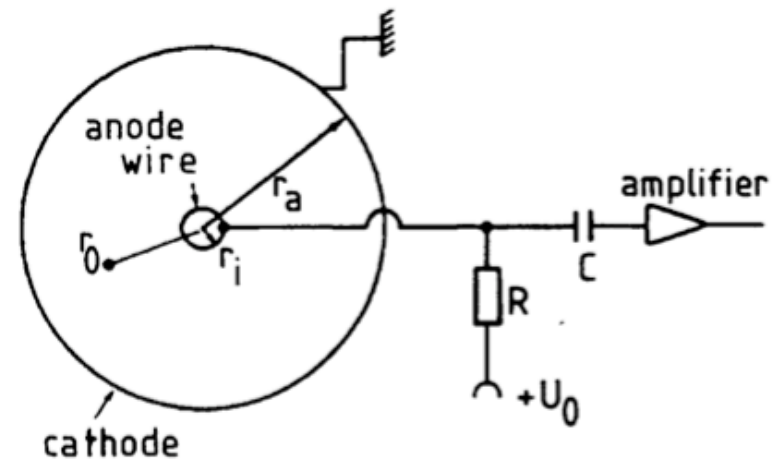
Ionization Chambers

- simplest Gas Detector
- Basically a Capacitor
- Also possible with liquids and solids



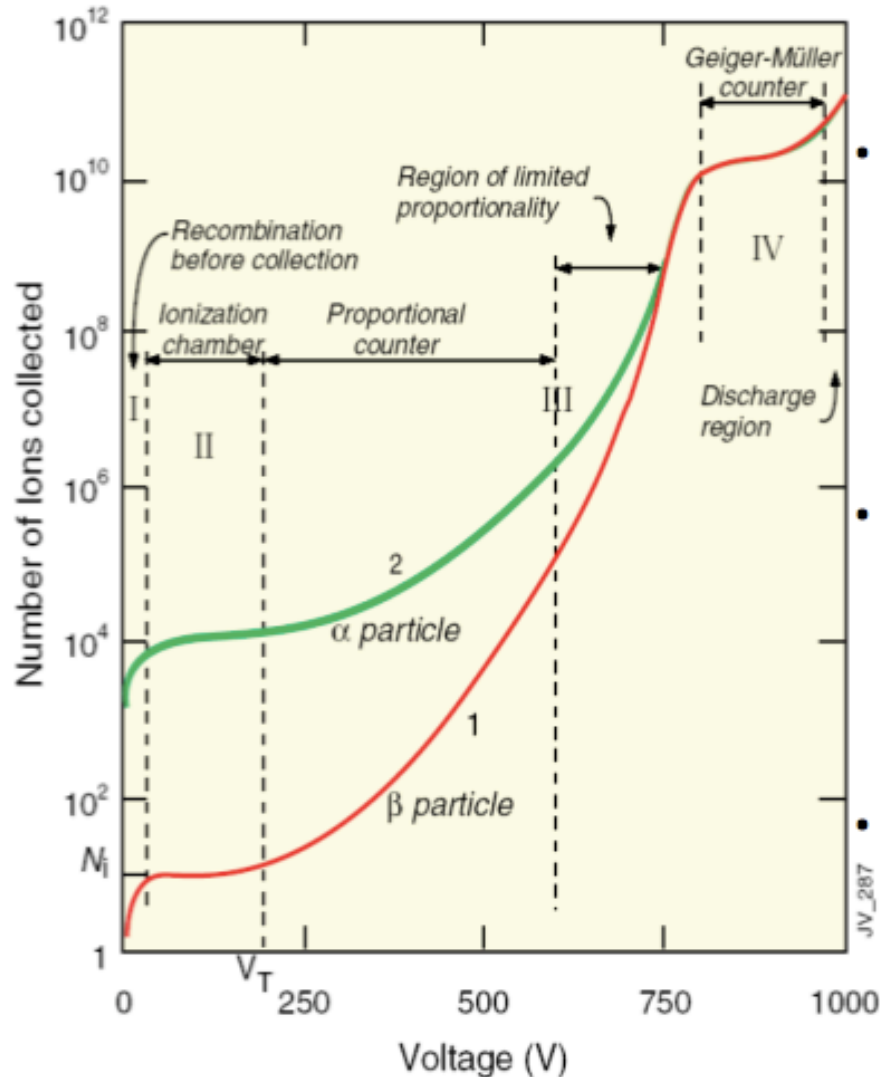
- Ionization (electrons and ions) drift to anode and cathode

If time constant of RC is large enough: Integrated signal \propto Ionization loss



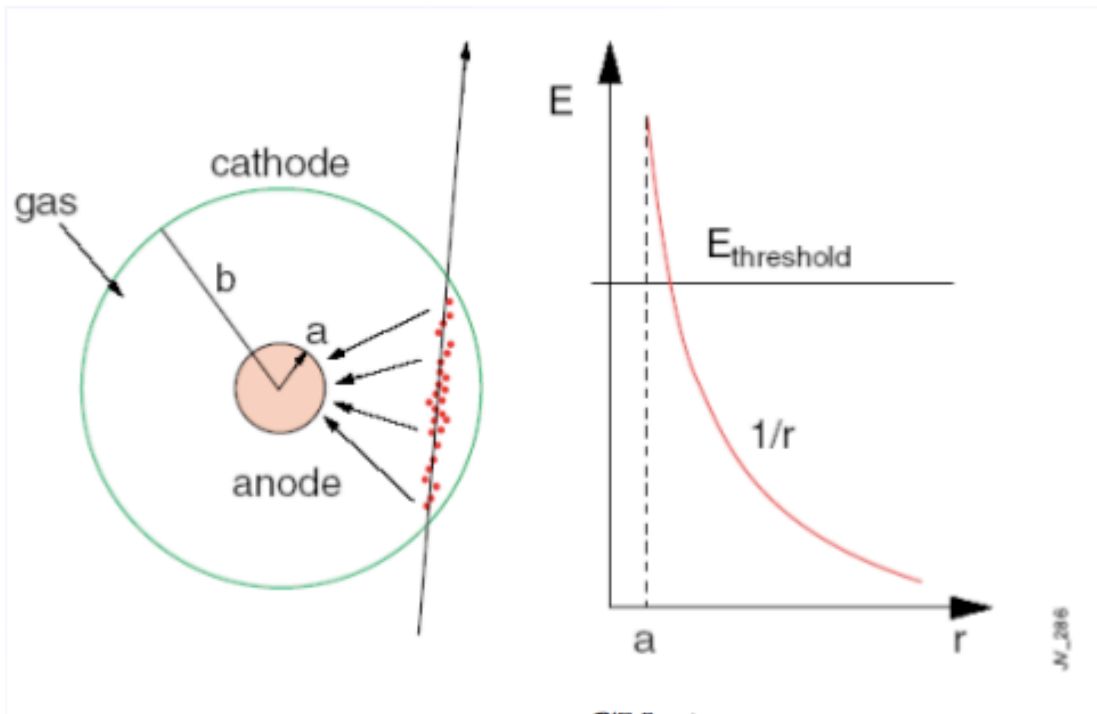
Ionization Chambers

SWPC OPERATION MODE



- ionization mode
 - full charge collection
 - no multiplication
 - gain ~ 1
- proportional mode
 - multiplication of ionization
 - signal proportional to ionization
 - measurement of dE/dx
 - secondary avalanches have to be quenched;
 - gain ~ 10⁴ – 10⁵
- limited proportional mode (saturated, streamer)
 - strong photoemission
 - secondary avalanches
 - requires strong quenchers or pulsed HV; gain ~ 10¹⁰
- Geiger mode
 - massive photoemission; full length of the anode wire affected;
 - discharge stopped by HV cut

Proportional Chamber: Single Wire



Electrons produced by **ionization** drift to the anode wire.

Avalanche:

- Close to the wire (\varnothing about few tens of μm) the E-field is very large ($> 10 \text{ kV/cm}$).
- Between collisions electrons gain enough energy to ionize gas.
- Exponential increase of number of electron/ion pairs (**gas amplification**)

$$n = n_0 e^{\alpha(E)x}$$

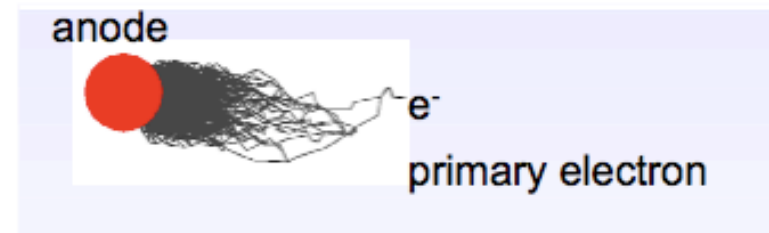
α is the first **Townsend coefficient**.

Electric field: $E(r) = \frac{CV_0}{2\pi\epsilon_0} \frac{1}{r}$

Potential: $V(r) = \frac{CV_0}{2\pi\epsilon_0} \ln \frac{r}{a}$

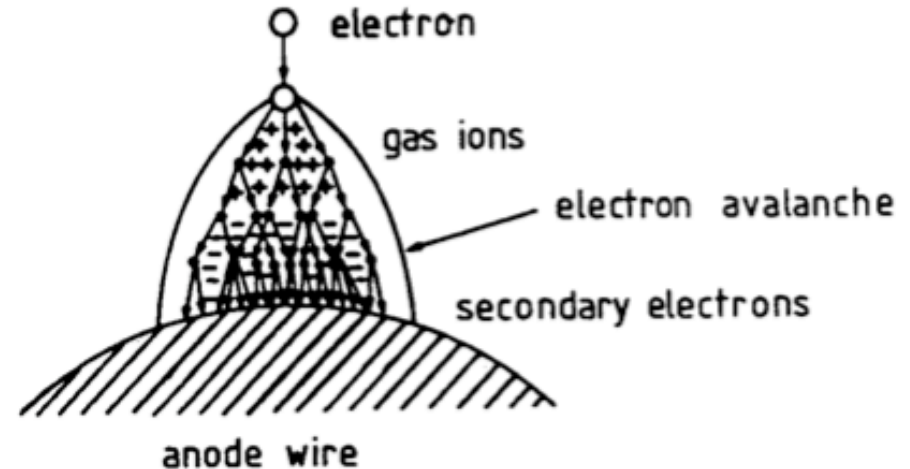
$V_0 =$ voltage between anode-cathode

Capacitance per length $C = \frac{2\pi\epsilon}{\ln(b/a)}$



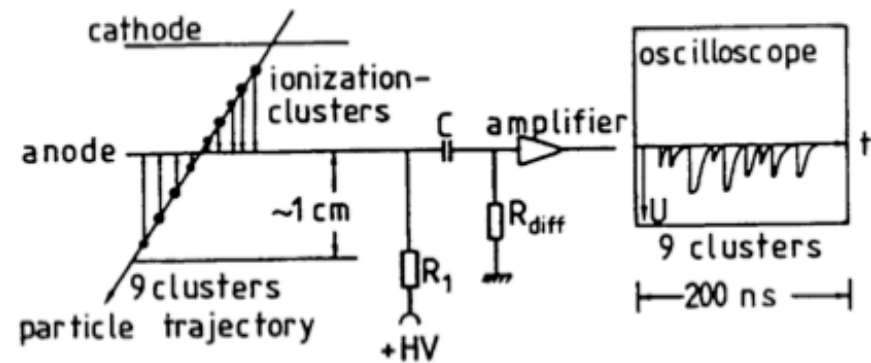
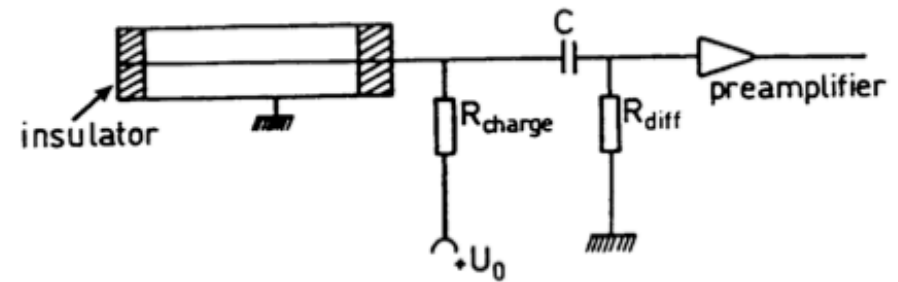
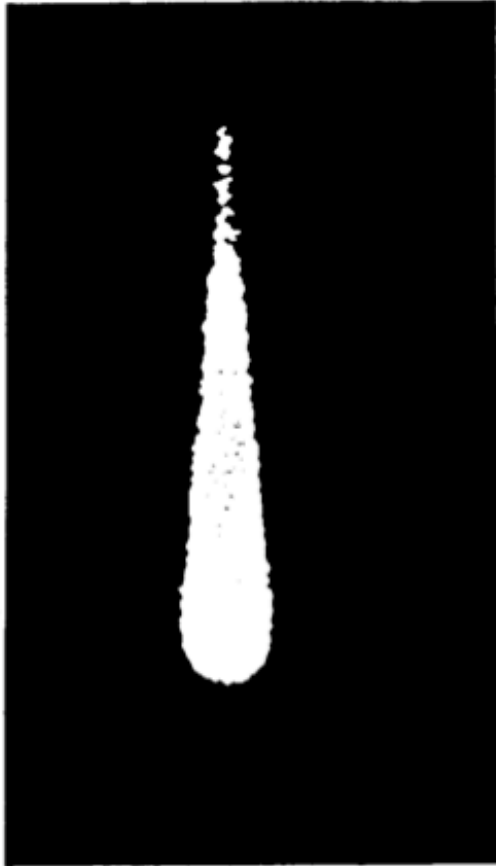
Proportional Chambers

- Like Ionization chamber, but smaller wire and/or higher voltage
- Charge multiplication close to wire ($E \propto 1/r$)
- Electrons gain enough energy between collisions to ionize themselves.

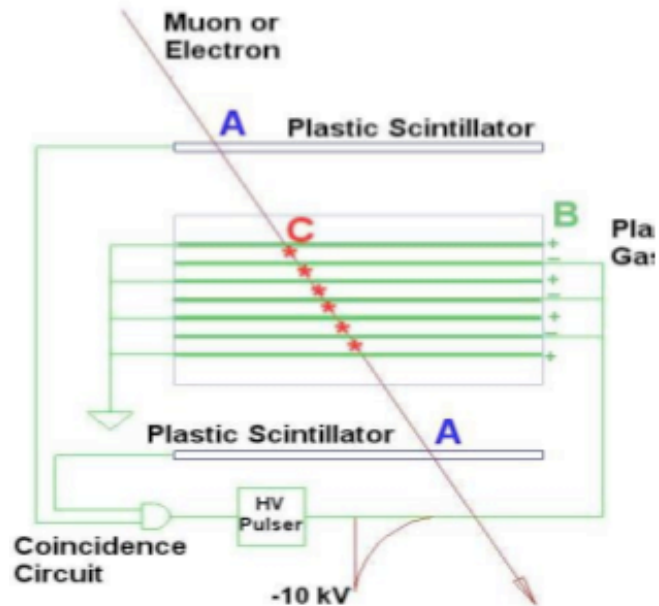


- Proportional: Gas amplification constant
→ Signal \propto primary ionization

Proportional Chambers



Spark Chamber

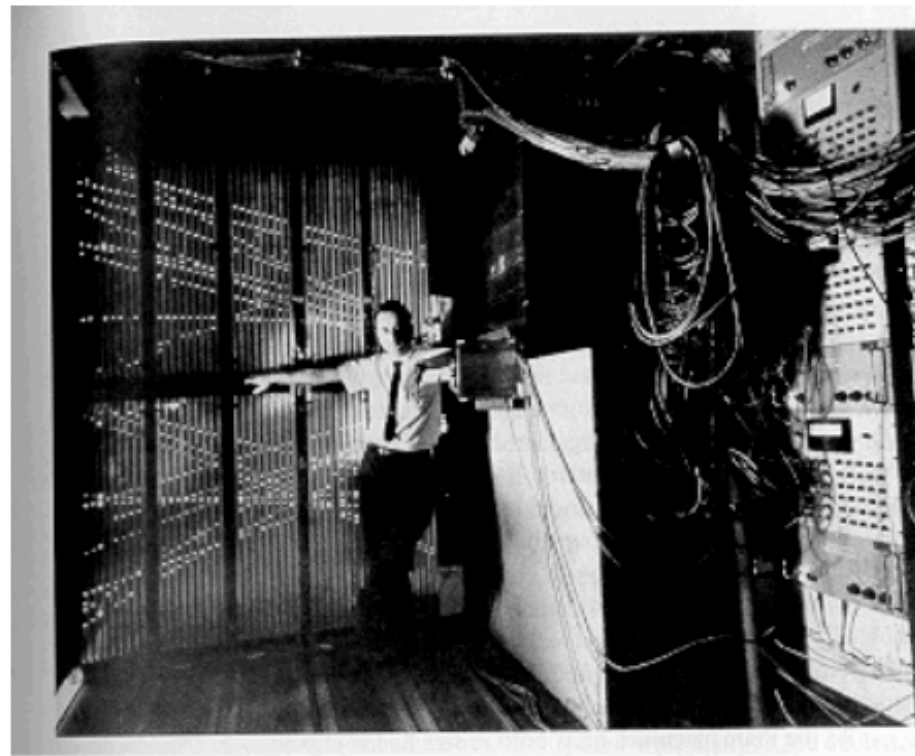


The Spark Chamber was developed in the early 60ies.

Schwartz, Steinberger and Lederman used it in discovery of the muon neutrino

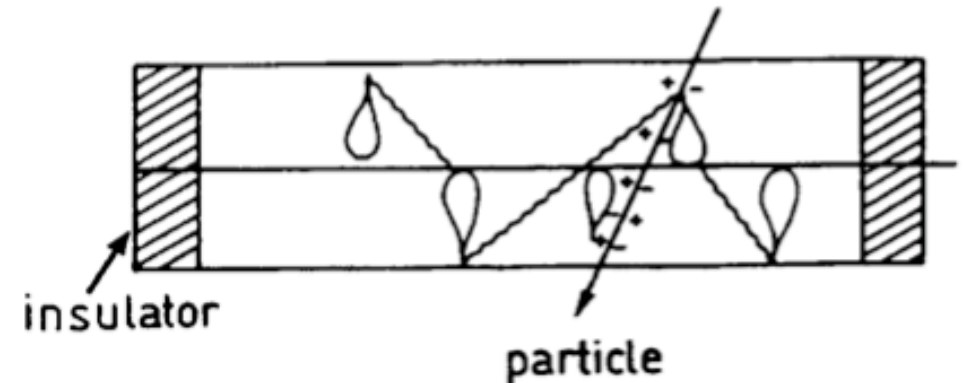
A charged particle traverses the detector and leaves an ionization trail.

The scintillators trigger an HV pulse between the metal plates and sparks form in the place where the ionization took place.

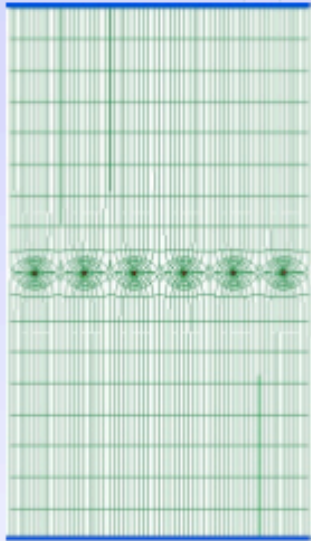


Geiger-Muller Counter

- Even higher voltage
- Copious production of photons in avalanche
- Photons make more ionization by photoelectric effect
- Also far away from original avalanche
- To stop discharge:
 - Make charge resistor big enough so voltage drops enough (quenching by resistor)
 - Add alcohols (methylal, ethylalcohol) or hydrocarbons (methane, ethane, isobutane) to counting gas (usually argon):
Absorb UV photons, reduce free path



Multi-Wire proportional Chamber



Simple idea to multiply SWPC cell : Nobel Prize 1992

First electronic device allowing high statistics experiments !!

Typical geometry
5mm, 1mm, 20 μm

Normally digital readout :
spatial resolution limited to

$$\sigma_x \approx \frac{d}{\sqrt{12}}$$

for d=1 mm
 $\sigma_x = 300 \mu\text{m}$

$$\langle x^2 \rangle = \frac{\int_0^{d/2} x^2 dx}{\int_0^{d/2} dx} = \frac{2}{d} \frac{x^3}{3} \Big|_0^{d/2} = \frac{d^2}{12}$$

from L. Ropelewski



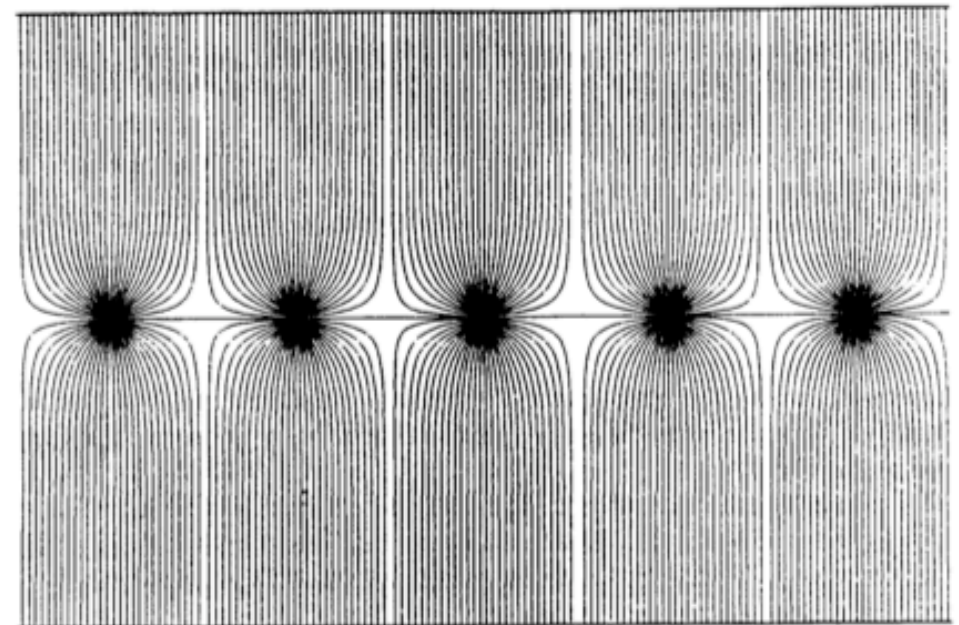
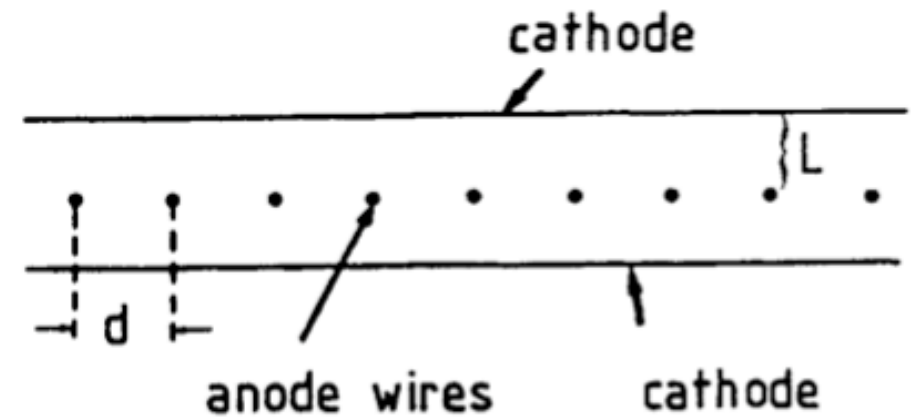
First large size MWPC



G. Charpak, F. Sauli and J.C. Santiard ,1970

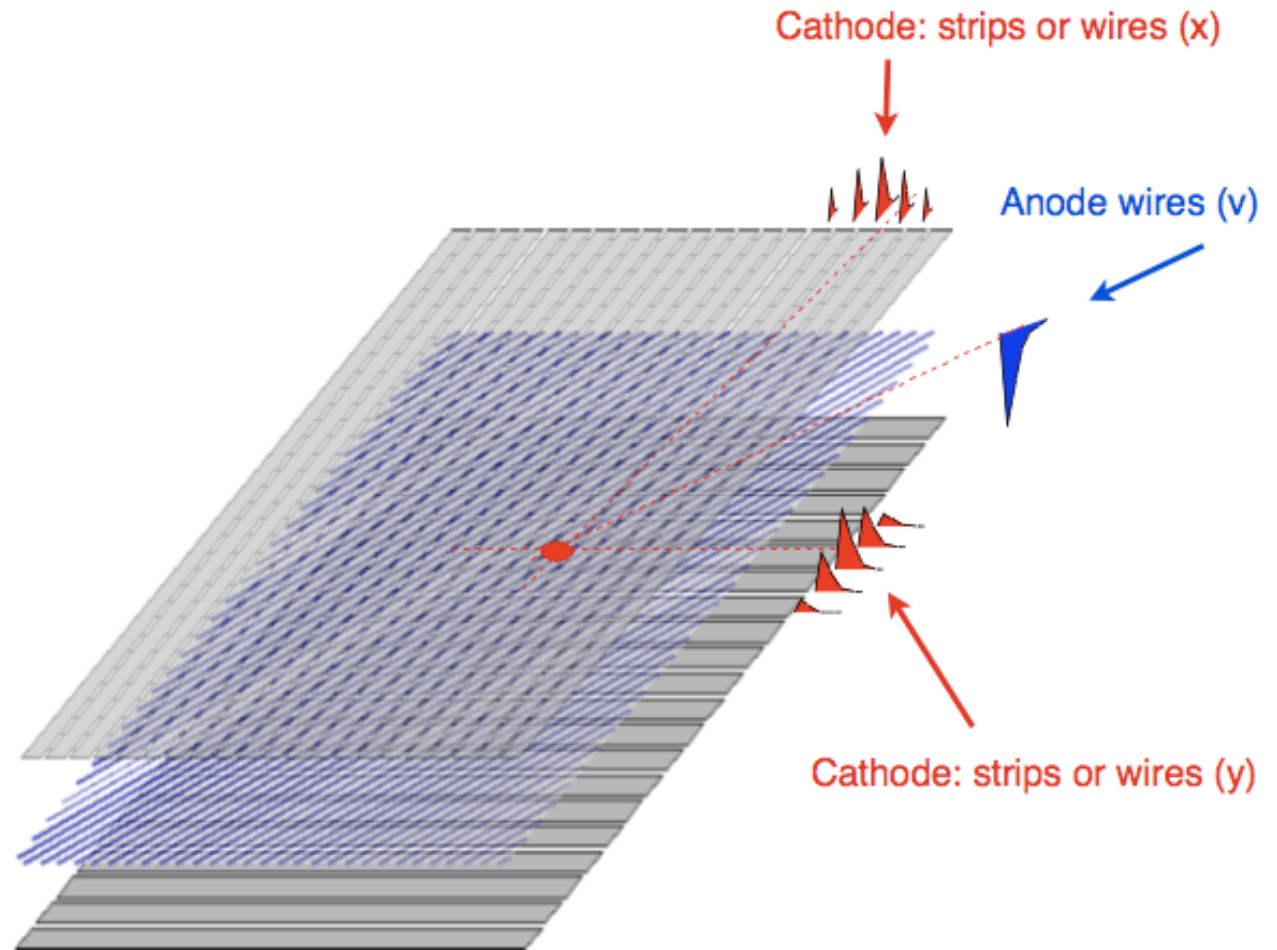
Multi-Wire Proportional Chambers

- George Charpak, beginning of 1960's, Nobel Price 1992
- Typical wire distance d : a few mm (> 0.8 mm)
- Typical wire diameter: $10\ \mu\text{m} - 30\ \mu\text{m}$
- Sizes: up to square meters. Limited by wire tension and electrostatic repulsion.
- Electronic: Discriminator (threshold).
- Resolution: $\sigma(x) = d/\sqrt{12}$
- space information only in one dimension
- Rotate second identical module for other dimension
- Segmented cathode readout for other dimension

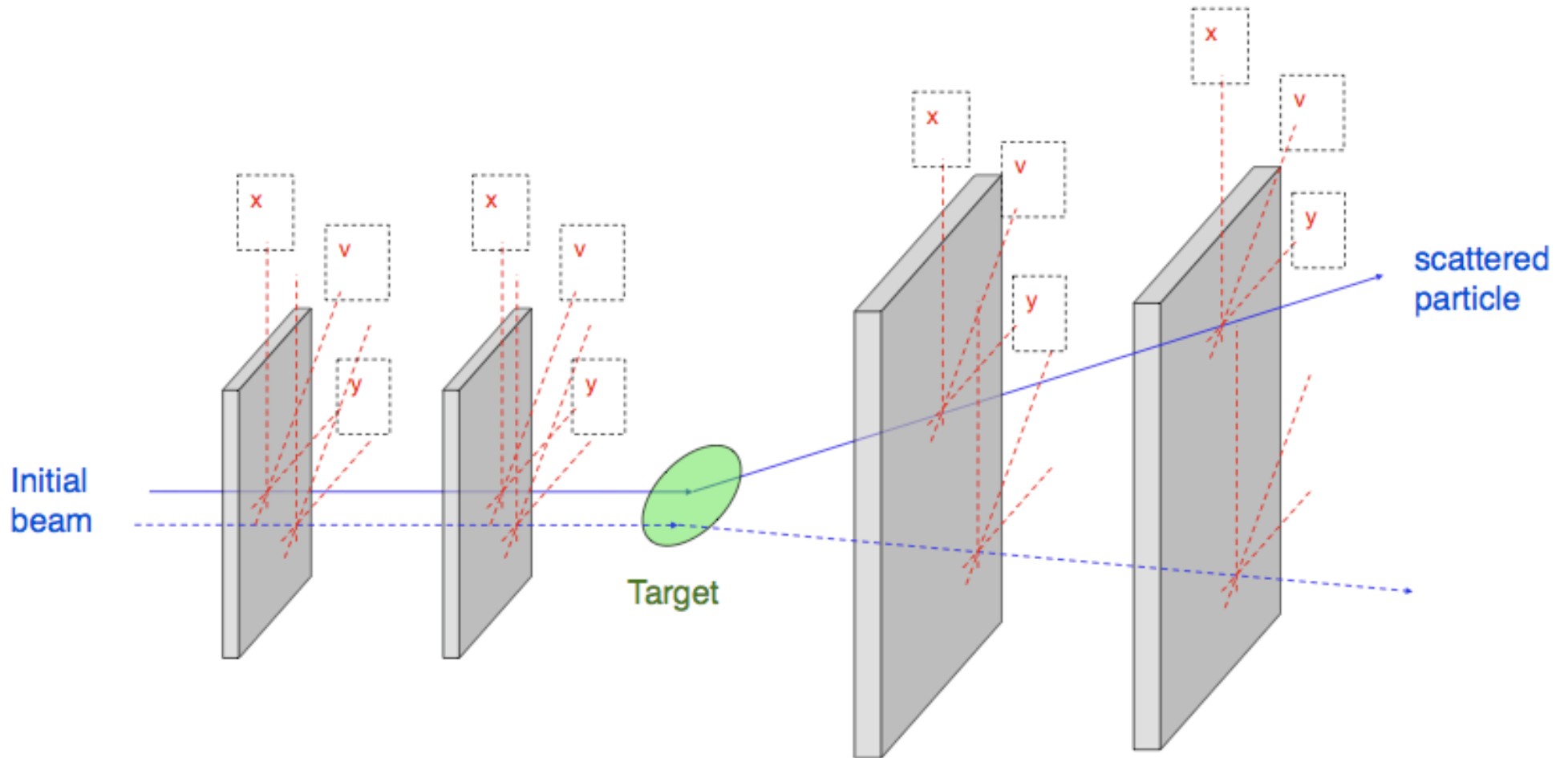


Multi-wire Proportional Chamber

Two coordinates (x,y) of the track hit can be determined from the position of the **anode wire** and the signal induced on the **cathode strips** (or wires).



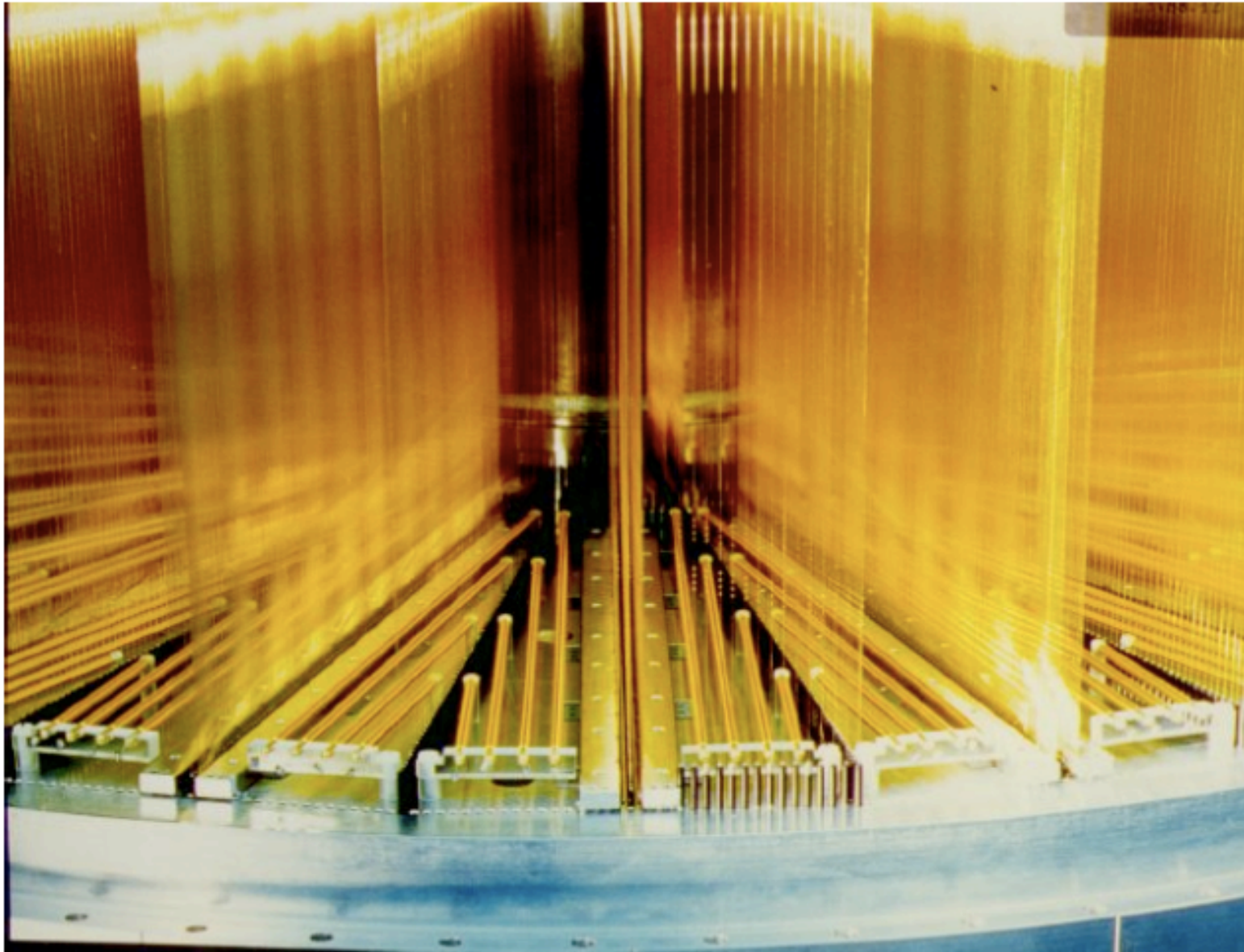
MWPC: Experimental set-up



With this experimental set-up based on MWPC an event rate of about 100 000 Hz can be processed. The position resolution in each layer is about 1 mm.

MWPC with many wire planes.

1985

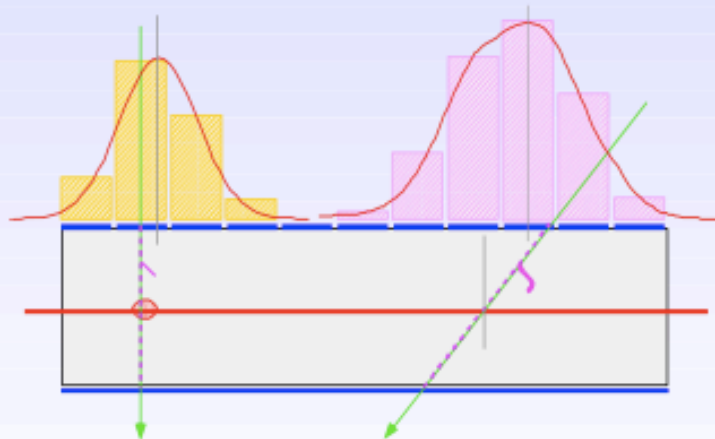




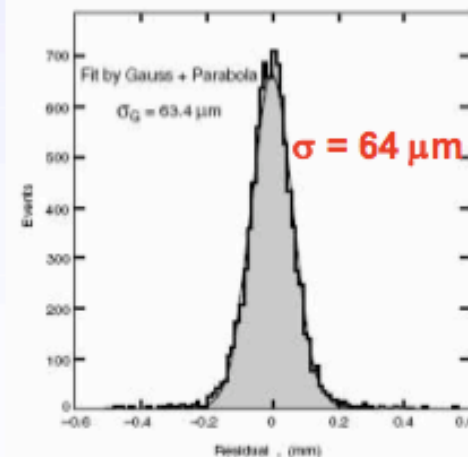
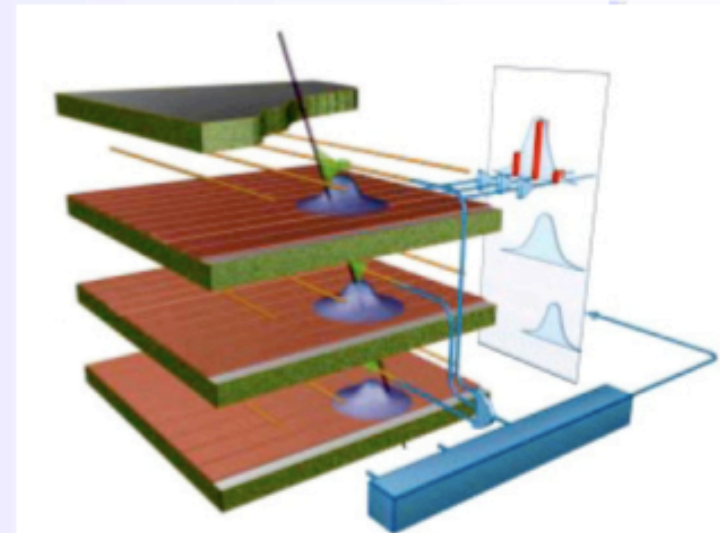
Cathode Strip Chambers

from L. Ropelewski

Precise measurement of the second coordinate by interpolation of the signal induced on pads.
Closely spaced wires makes CSC fast detector.



Center of gravity of induced signal method.



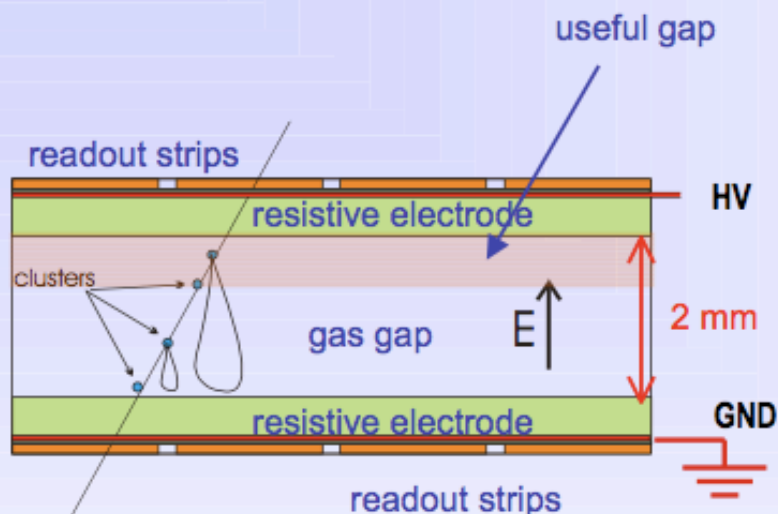
Space resolution



CMS

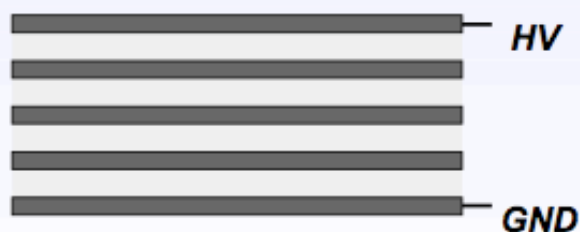
Resistive Plate Chambers

from L. Ropelewski



Rate capability strong function of the resistivity of electrodes in streamer mode.

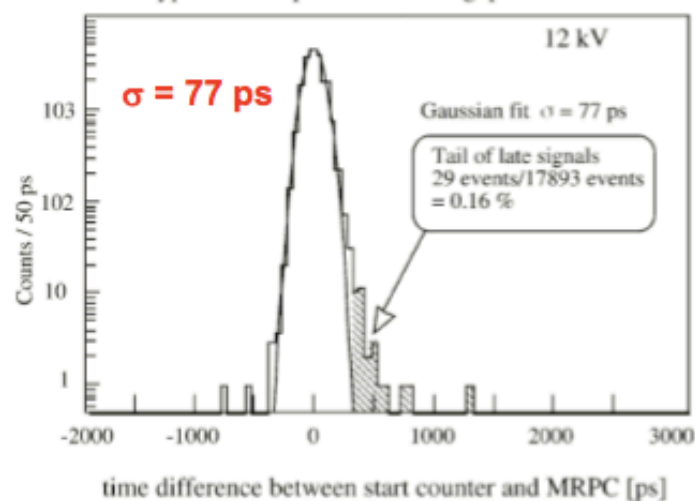
MRPC



Multigap RPC - exceptional time resolution suited for the trigger applications

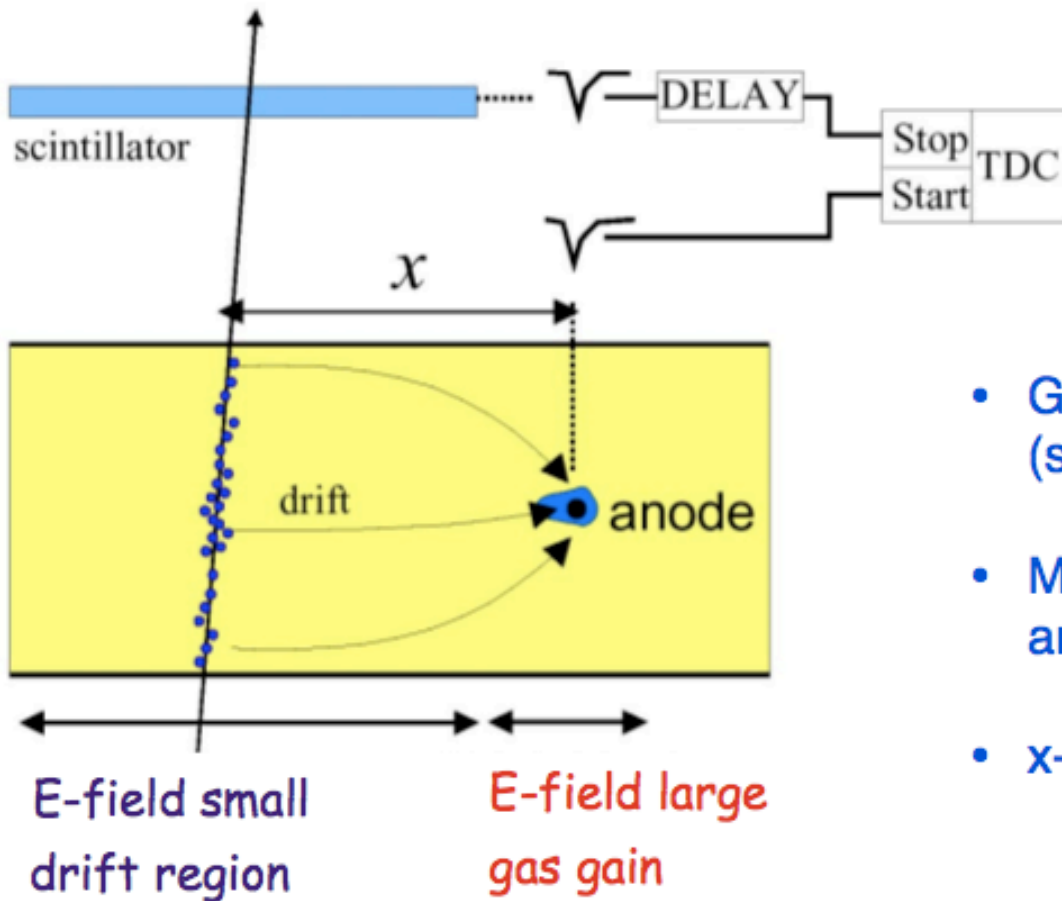
A. Akindinov et al., NIM A456(2000)16

Typical time spectrum from 5 gap MRPC



Time resolution

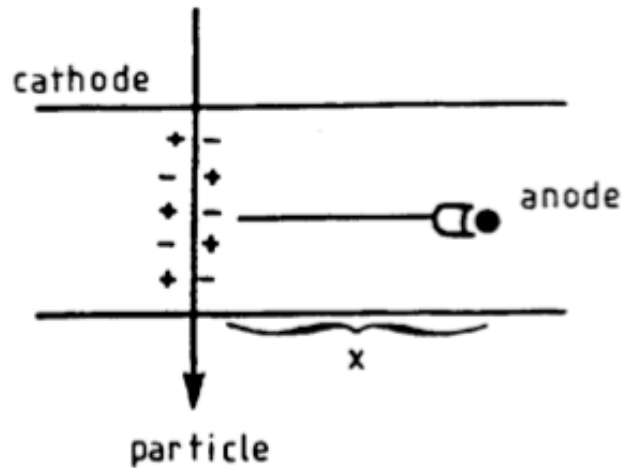
Driftchamber



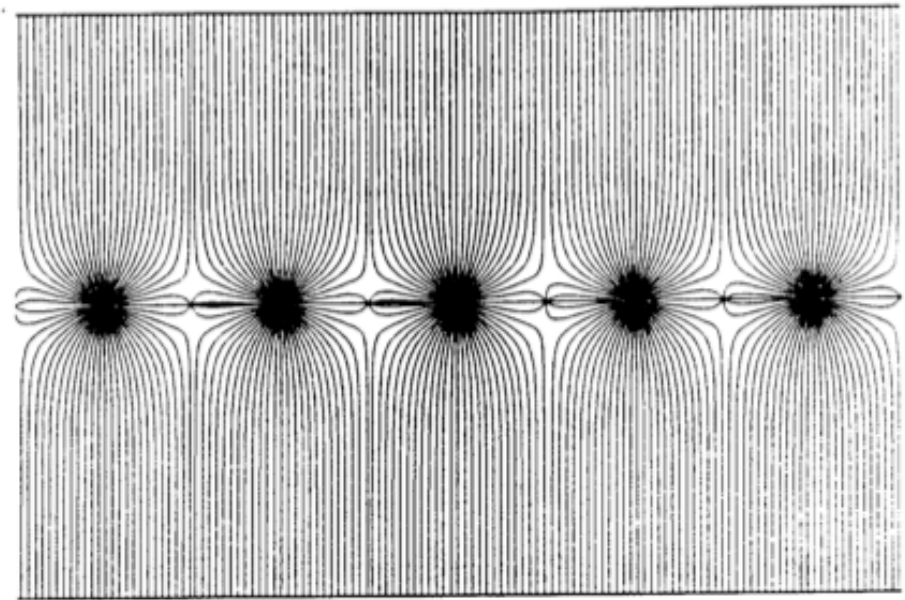
TDC: Time to Digital Converter

- Get external time reference t_0 (scintillator)
- Measure arrival time of electrons at anode t_1
- x- coordinate given by $x = \int_{t_0}^{t_1} v_D(t) dt$
- advantage of drift chamber: much larger sensitive volume per readout channel.

Planar Drift Chambers

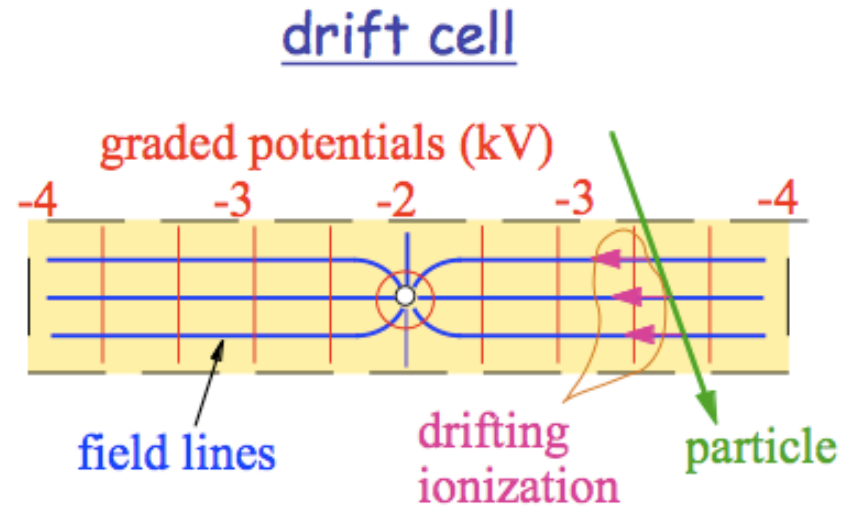


- Heintze, Walenta, \approx 1968, also others.
- Make wires further apart
- use drift time to wire as additional information
- additional potential wire
- drift distances several cm
- resolution: limited by diffusion.
small chambers: $\sigma > 20 \mu\text{m}$
larger chambers a few $100 \mu\text{m}$

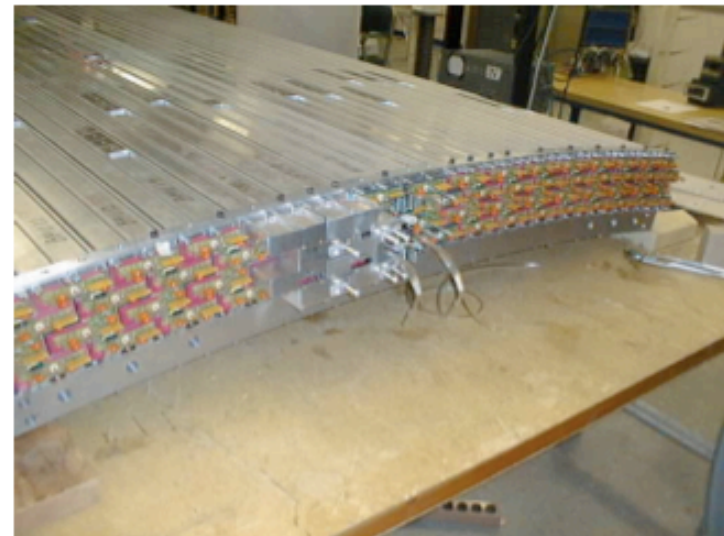


Driftchamber

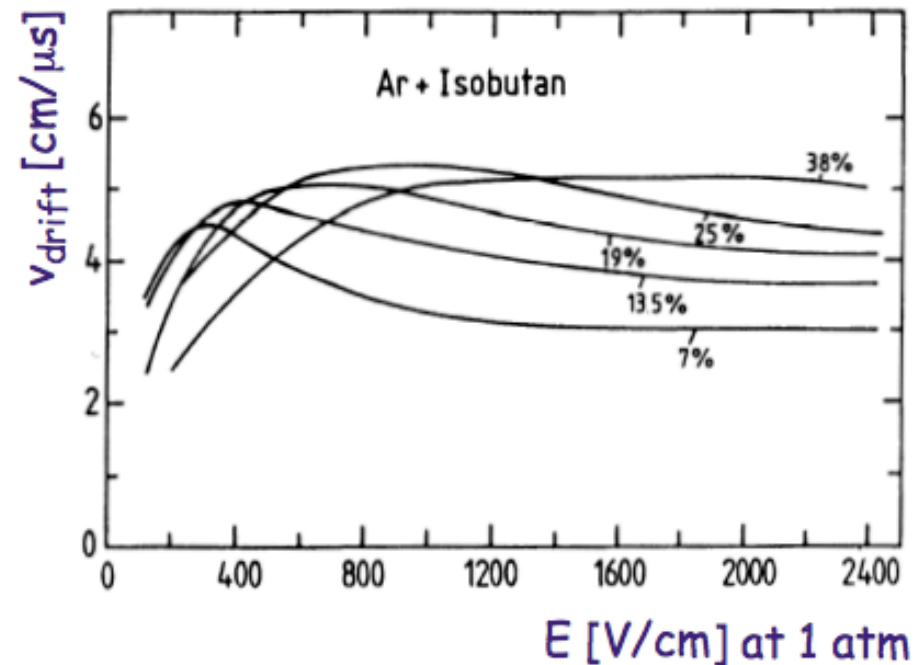
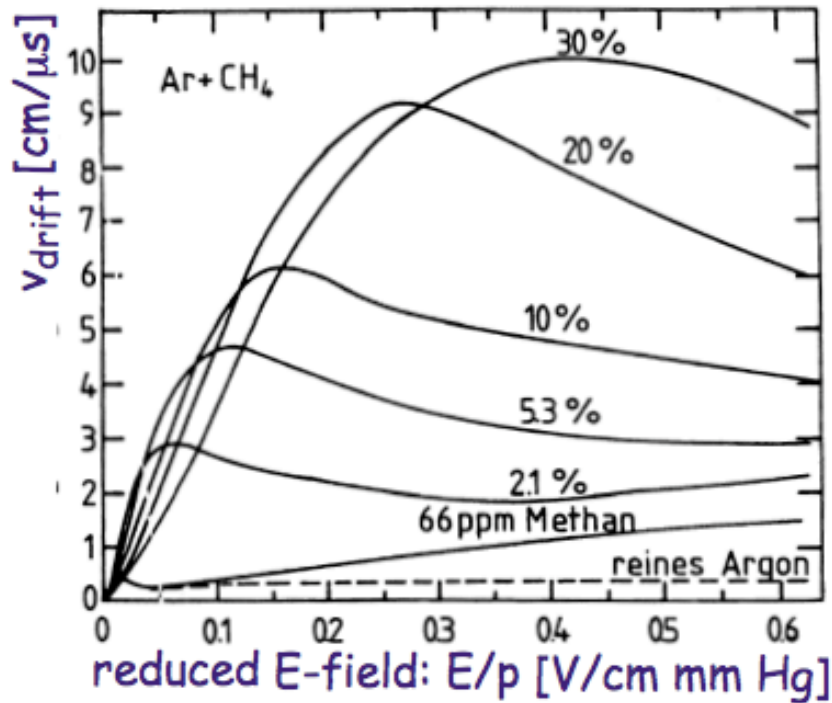
- Use graded potential to get uniform drift field.
- Gas amplification near anode wire.
- Position resolution ($\sigma = 50 - 200 \mu\text{m}$)
 - $v(t)$ distortions near wire
 - ionisation fluctuations
 - diffusion
 - electronic noise



CDF muon chambers



Driftchamber: Drift Velocity



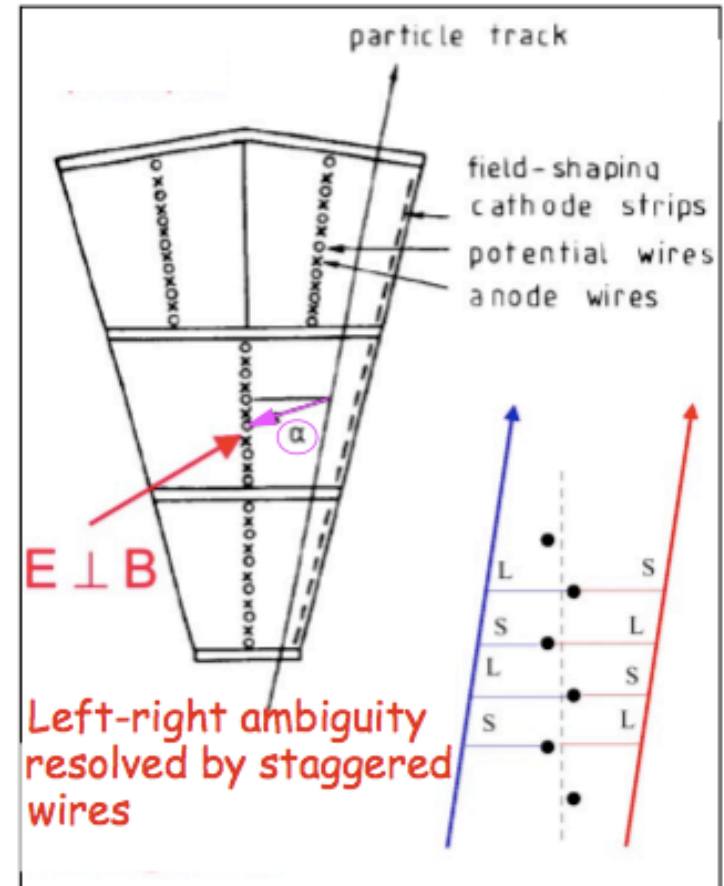
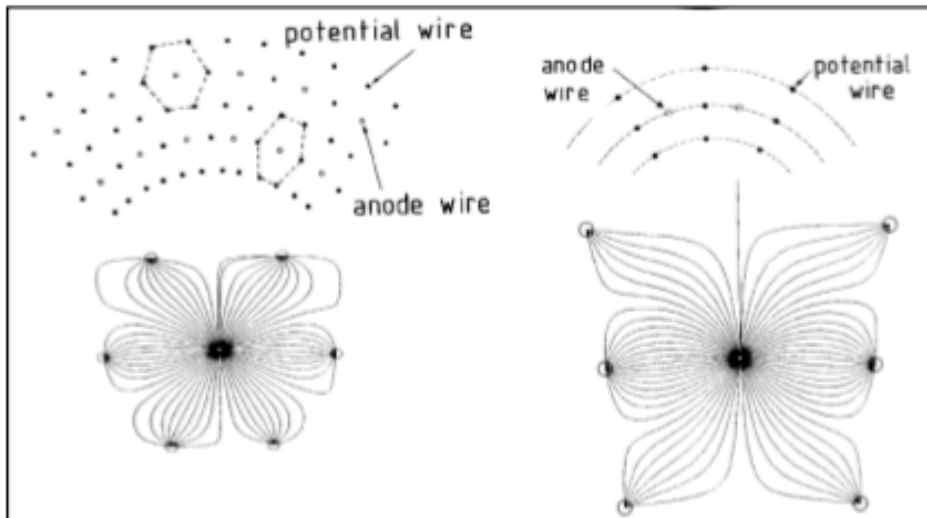
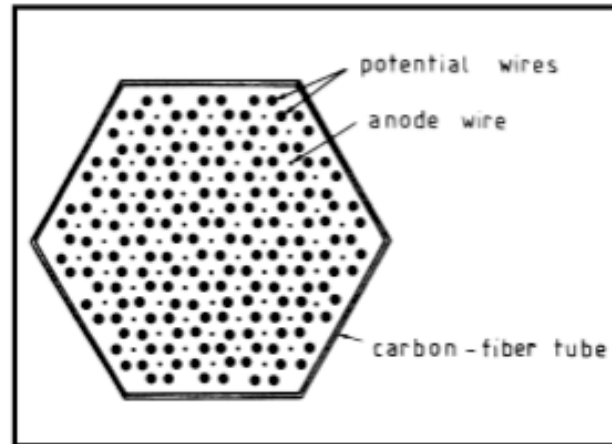
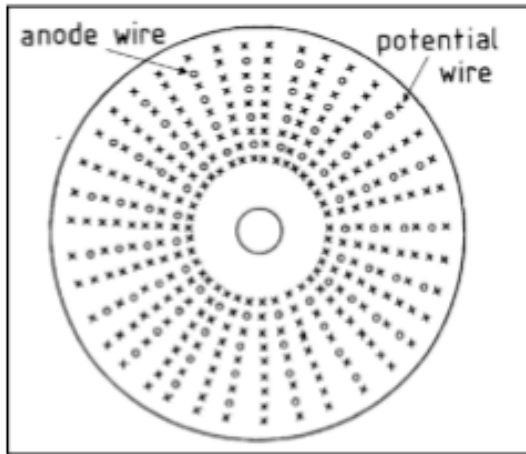
Some gas mixtures have a strong variation of drift velocity as function of E-field.

For stable operation it is useful to operate at maximum / plateau.

Typical drift velocities: 2-10 cm/ μs :

;

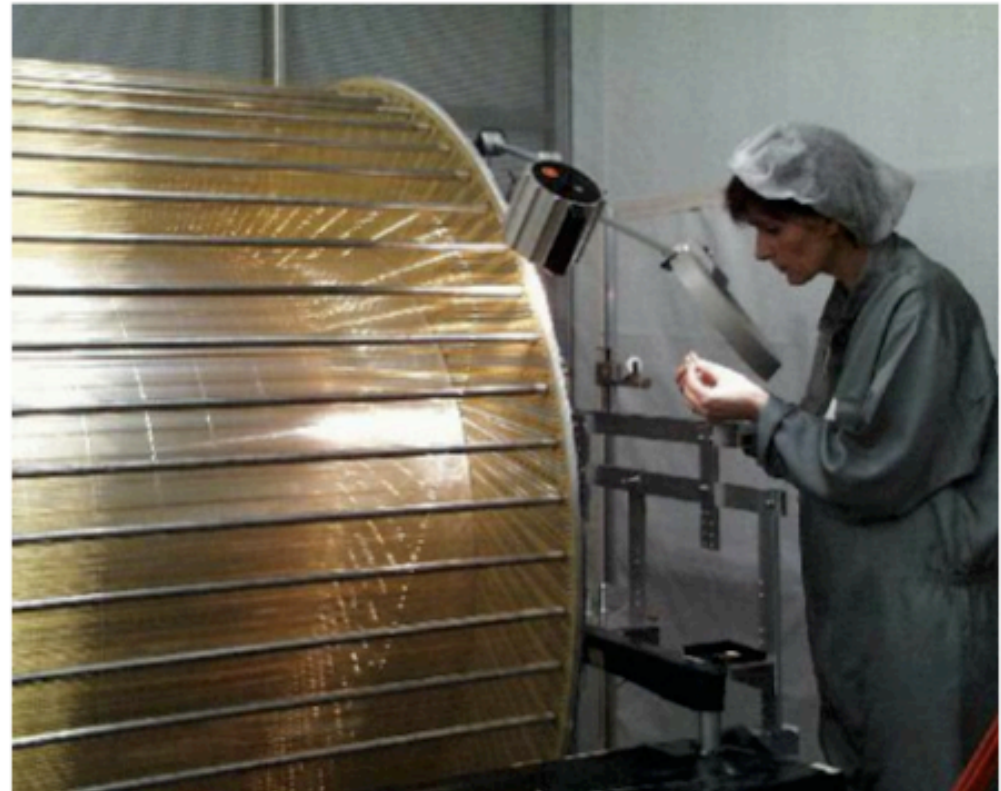
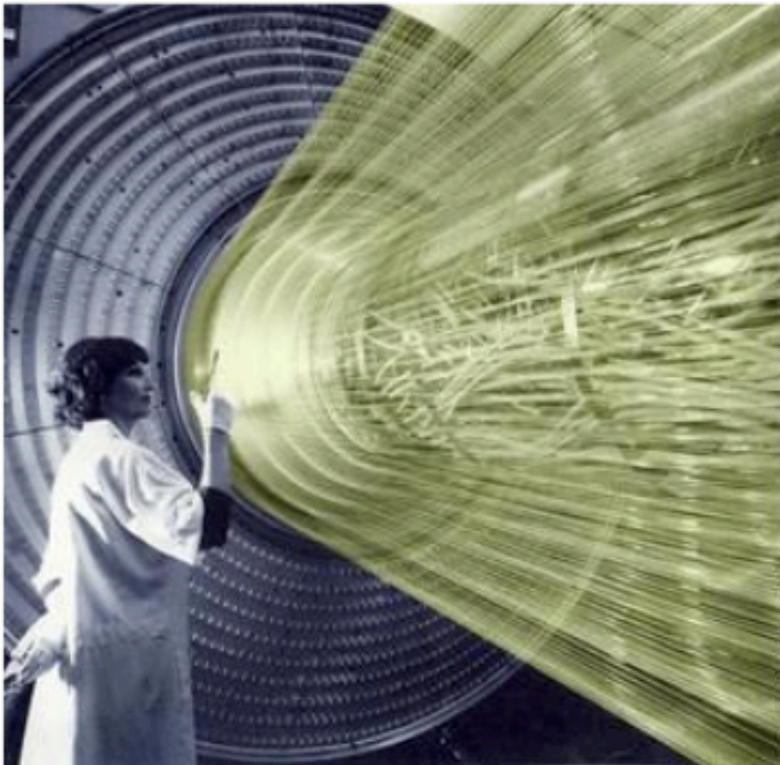
Cylindrical Drift Chamber



cell of a "jet"-driftchamber

Cylindrical Drift Chamber

H1 Central Jet Chamber



- ≈ 15000 wires
- total force from wire tension ≈ 6 tons

The ATLAS Muon Spectrometer

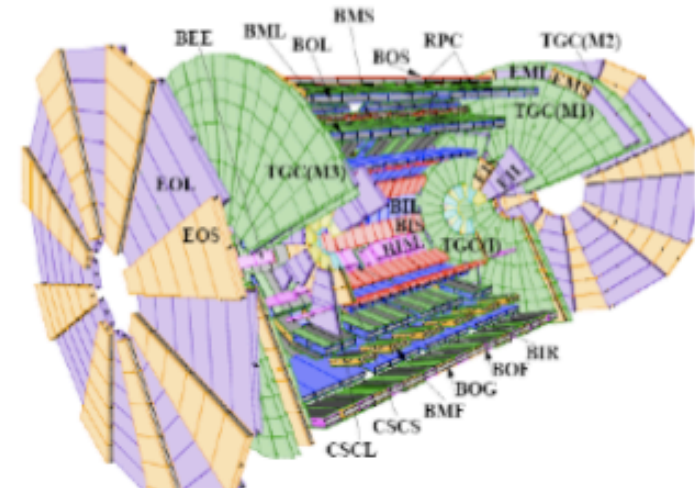
Monitored drift tubes - Coverage - Number of chambers - Number of channels - Function	MDT $ \eta < 2.7$ (innermost layer: $ \eta < 2.0$) 1088 (1150) 339 000 (354 000) Precision tracking
Cathode strip chambers - Coverage - Number of chambers - Number of channels - Function	CSC $2.0 < \eta < 2.7$ 32 31 000 Precision tracking
Resistive plate chambers - Coverage - Number of chambers - Number of channels - Function	RPC $ \eta < 1.05$ 544 359 000 Triggering, second coordinate
Thin gap chambers - Coverage - Number of chambers - Number of channels - Function	TGC $1.05 < \eta < 2.7$ (2.4 for triggering) 3588 318 000 Triggering, second coordinate

A complex system:

4 different technologies
(MDT,CSC,RPC,TGC)

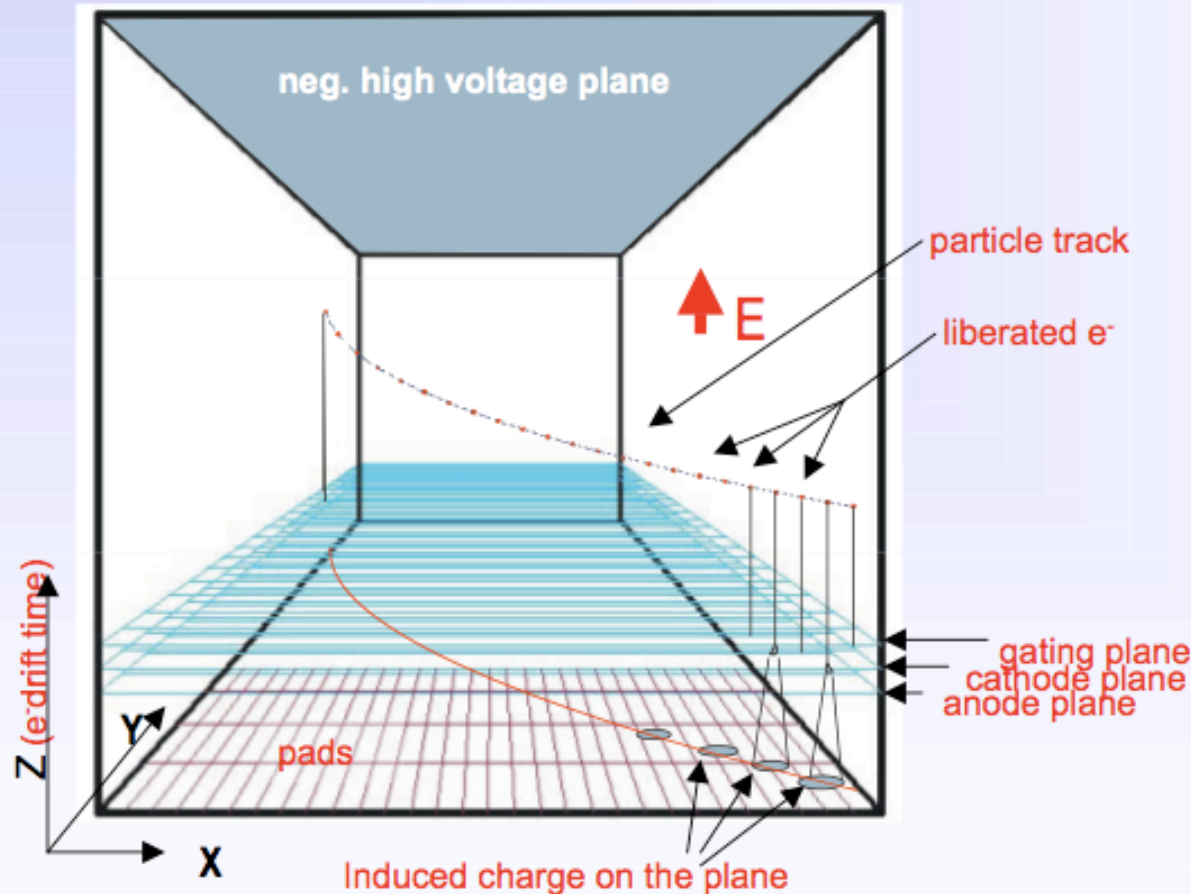
Large area (10,000 m²)

Many channels (1M)



Time Projection Chamber (TPC)

from L. Ropelewski



Time Projection Chamber
full 3D track reconstruction:
x-y from wires and segmented
cathode of MWPC (or GEM)
z from drift time

- **momentum** resolution
space resolution + B field
(multiple scattering)
- **energy** resolution
measure of primary ionization

TPC Time Projection Chamber

Developed by D. Nygren in the 70's.

Large gas volume with **central electrode**.

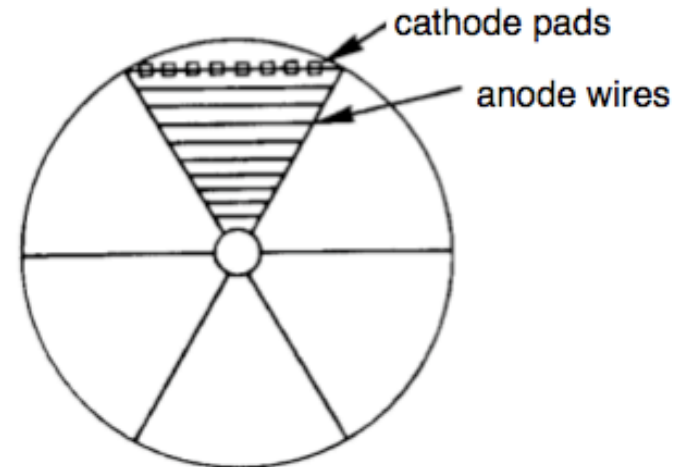
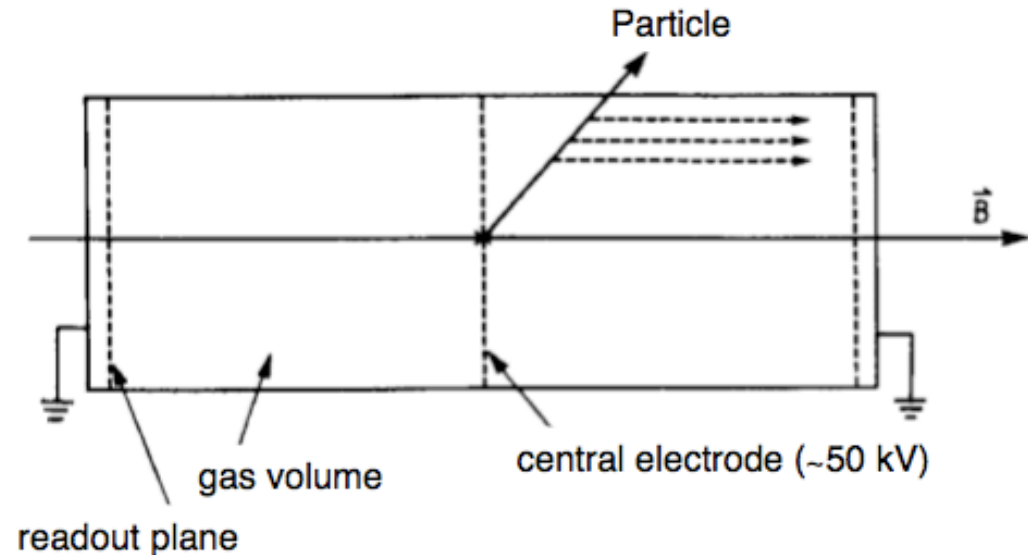
Drift distance of several meters.

Signal registered with **MWPC**, anode wires and cathode pads provide **x,y** ; drift time gives **z**.

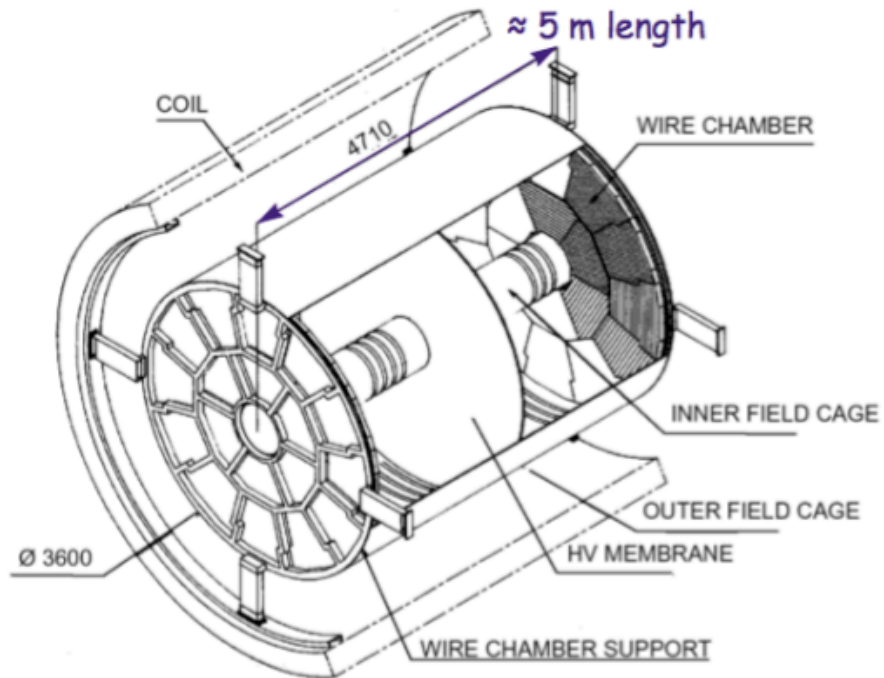
Transverse diffusion reduced (electrons spiral around E-field, since $E \parallel B$, Larmor radius $< 1 \mu\text{m}$)

Very good **3D hit resolution** and **dE/dx**.

Long drift times ($\approx 40 \mu\text{s}$), thus **rate limitations** and **very good gas quality** required.



ALEPH TPC at LEP

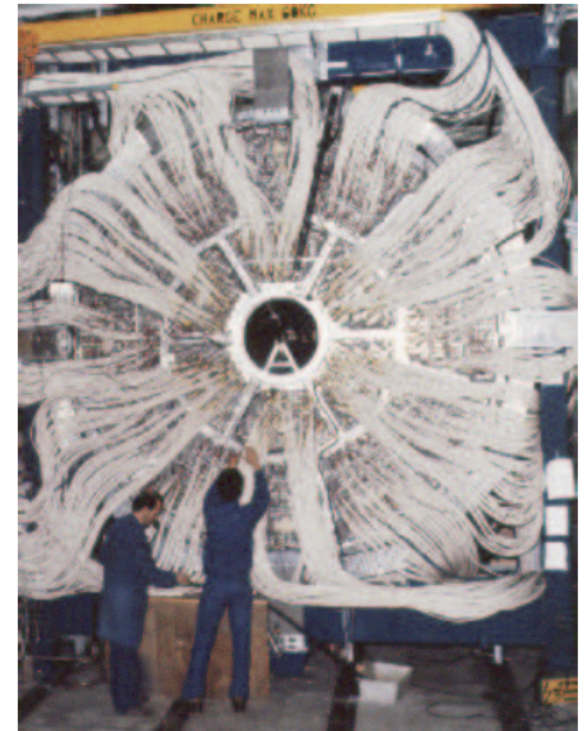
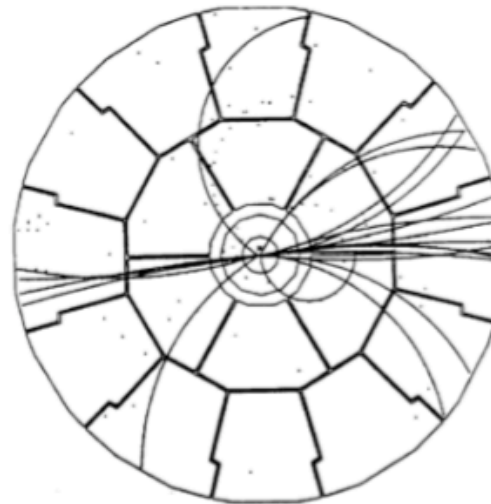


achieved resolutions:

$$\sigma_{r\phi} = 170 \mu\text{m}$$

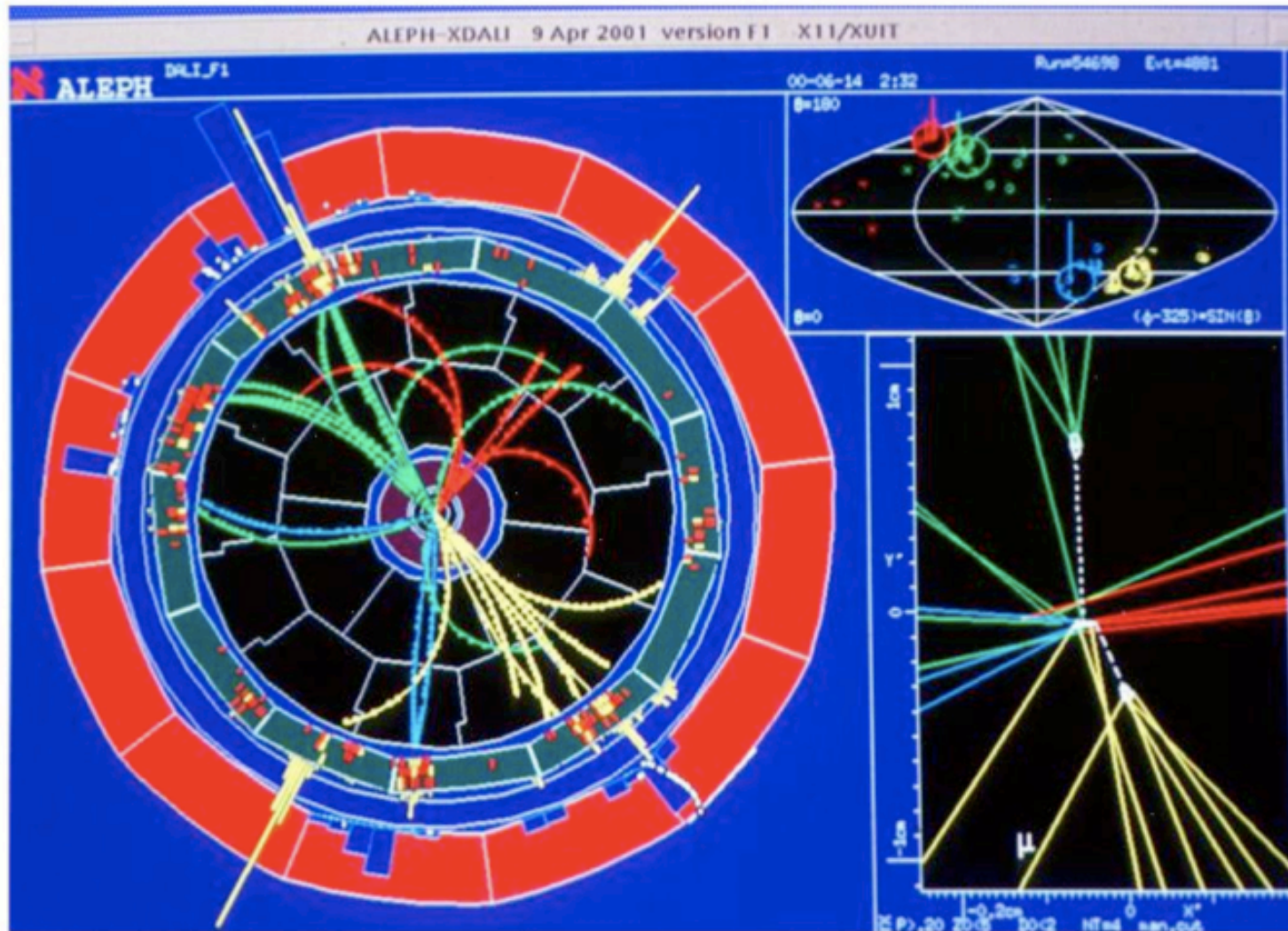
$$\sigma_z = 740 \mu\text{m}$$

r - ϕ projection



ALEPH TPC at LEP

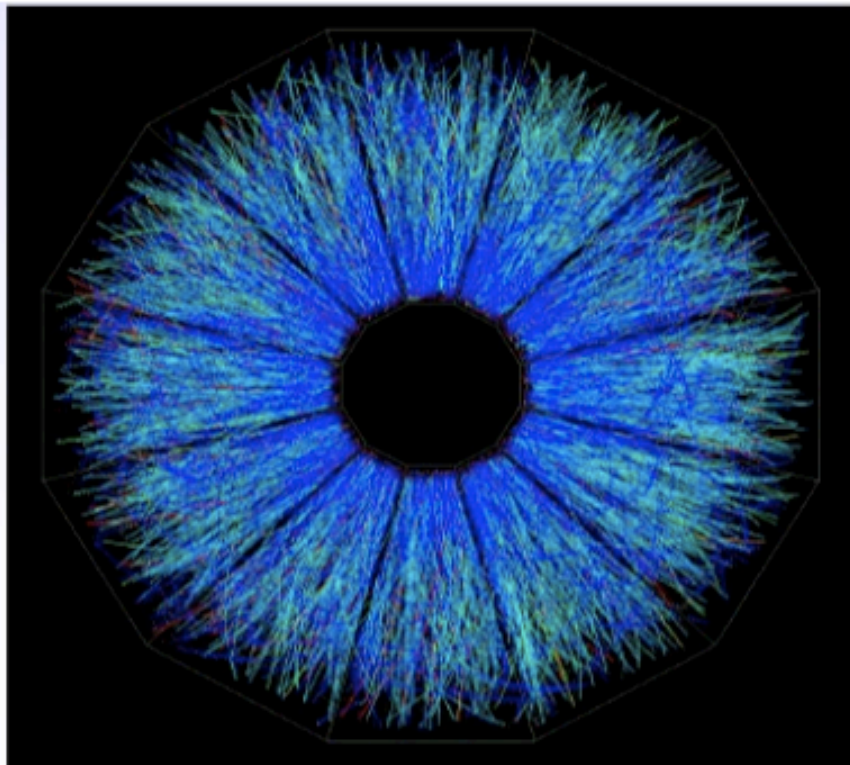
Aleph Higgs Candidate Event: $e^+ e^- \rightarrow HZ \rightarrow bb + jj$



TPC for Heavy Ion Collisions

Au+ Au+ collision in the
STAR Experiment/RHIC

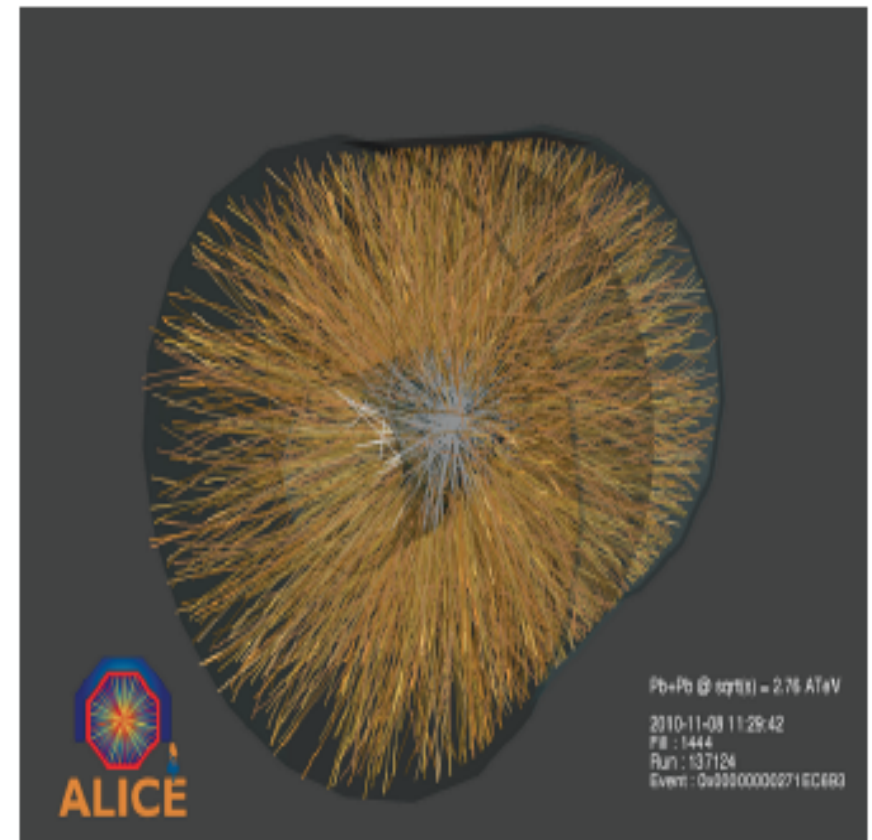
Up to 2000 tracks



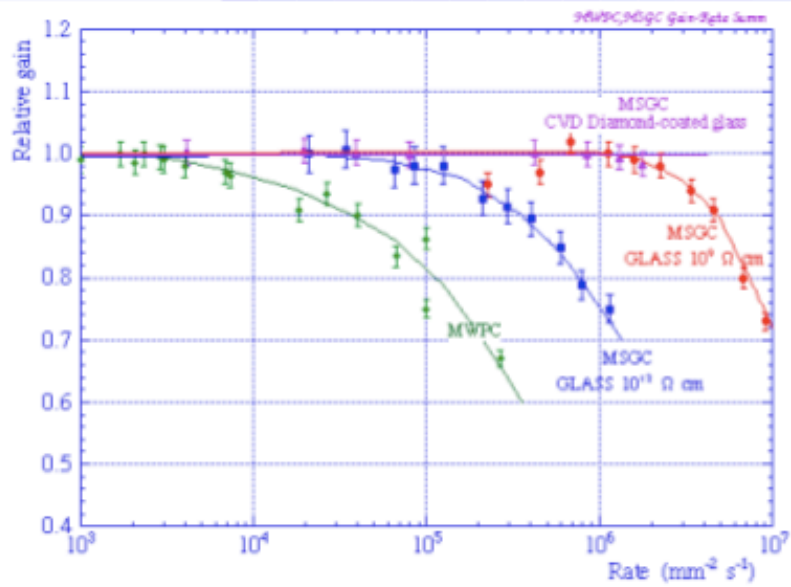
Pb+ Pb+ Kollision in the ALICE
Experiment/LHC

Angle $\Theta=60$ to 62°

Up to 40 000 tracks/collision



Micropattern Gas Chambers



Advantages of gas detectors:

- low radiation length
- large areas at low price
- flexible geometry
- spatial, energy resolution ...

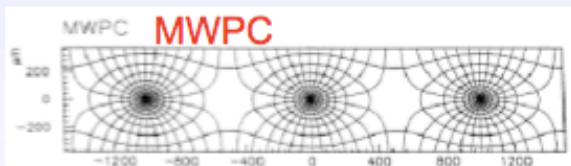
from L. Ropelewski

Problem:

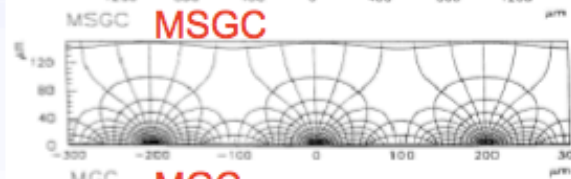
- rate capability limited by space charge defined by the time of evacuation of positive ions

scale factor

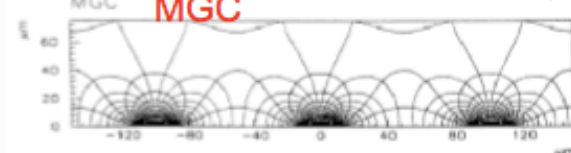
1



5



10

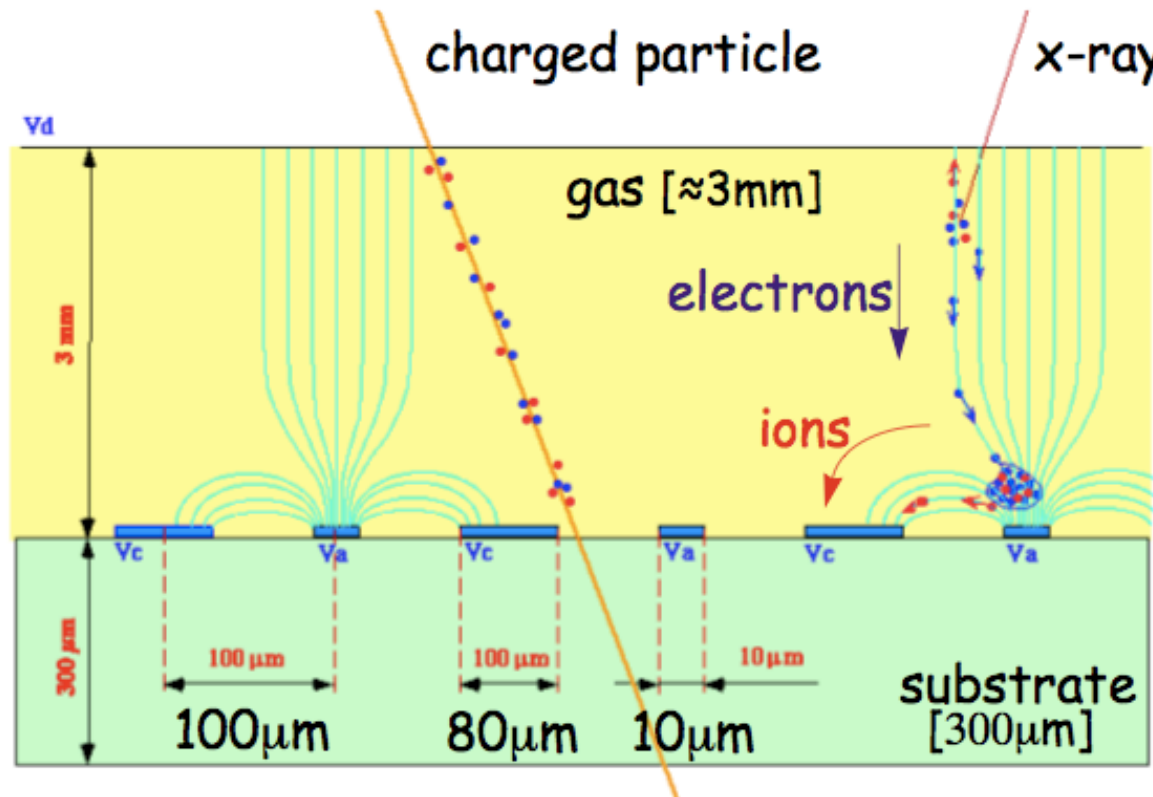


R. Bellazzini et al.

Solution:

- reduction of the size of the detecting cell (limitation of the length of the ion path) using chemical etching techniques developed for microelectronics and keeping at same time similar field shape.

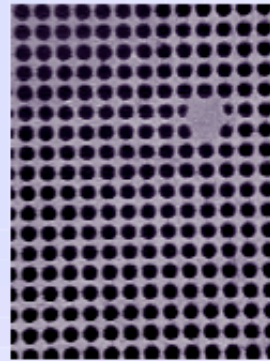
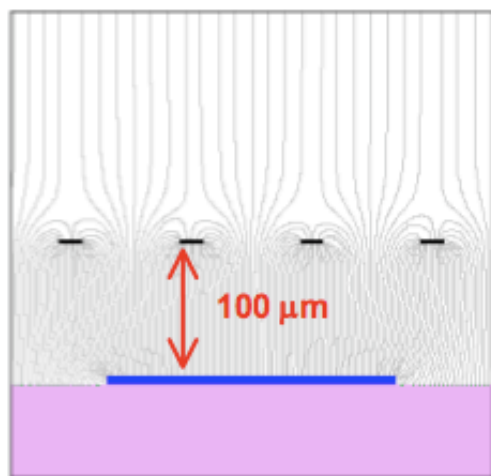
Microstrip Gas Chamber



Advantages:

- Very precise and small anode/cathode structures can be produced with lithographical methods. Thus very good position resolution is possible.
- MSGC provide high mechanical stability
- small drift distance for ions, thus high rate capability.

Micromegas: Micromesh Gaseous Structure

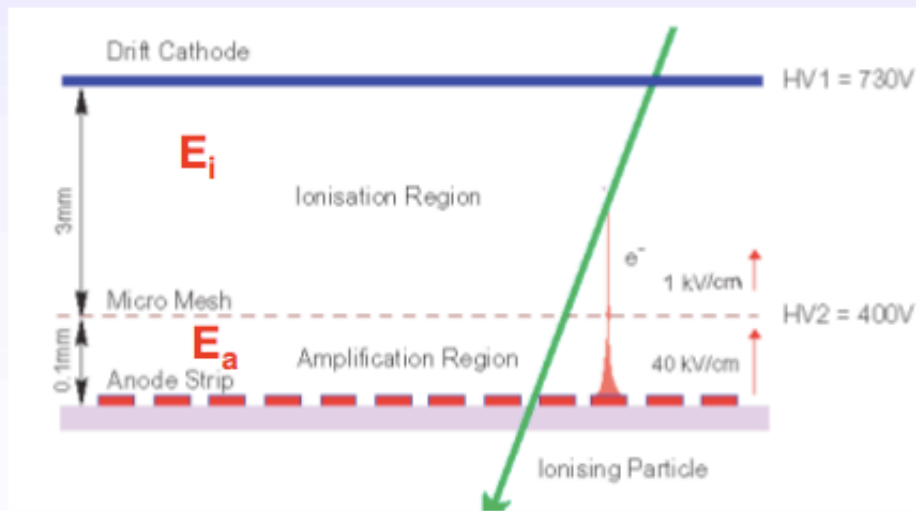


micromesh

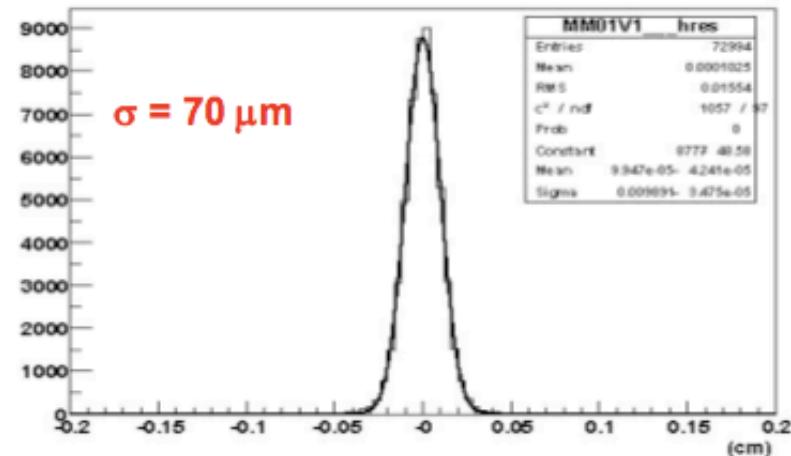
Micromesh mounted above readout structure (typically strips).

E field similar to parallel plate detector.

$E_a/E_i \sim 50$ to secure electron transparency and positive ion flowback suppression.

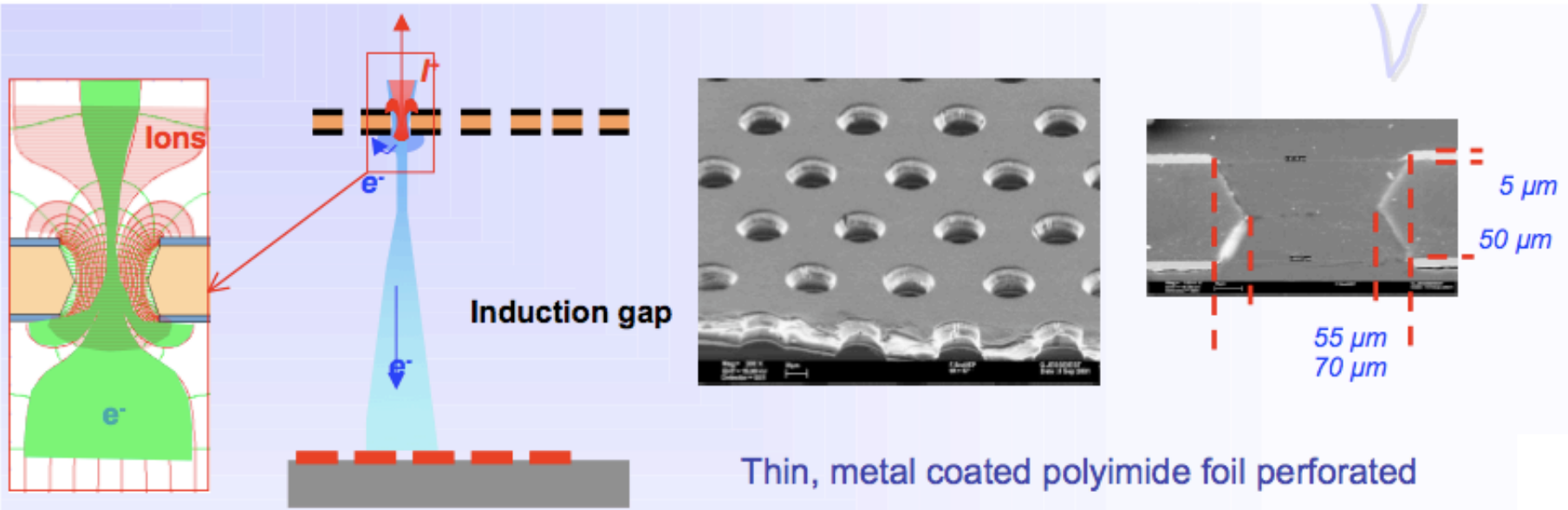


MM01V1_ Residuals

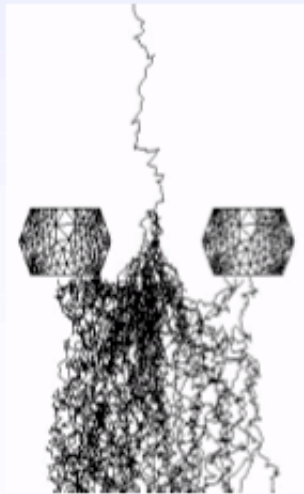


Space resolution

Gas Electron Multiplier

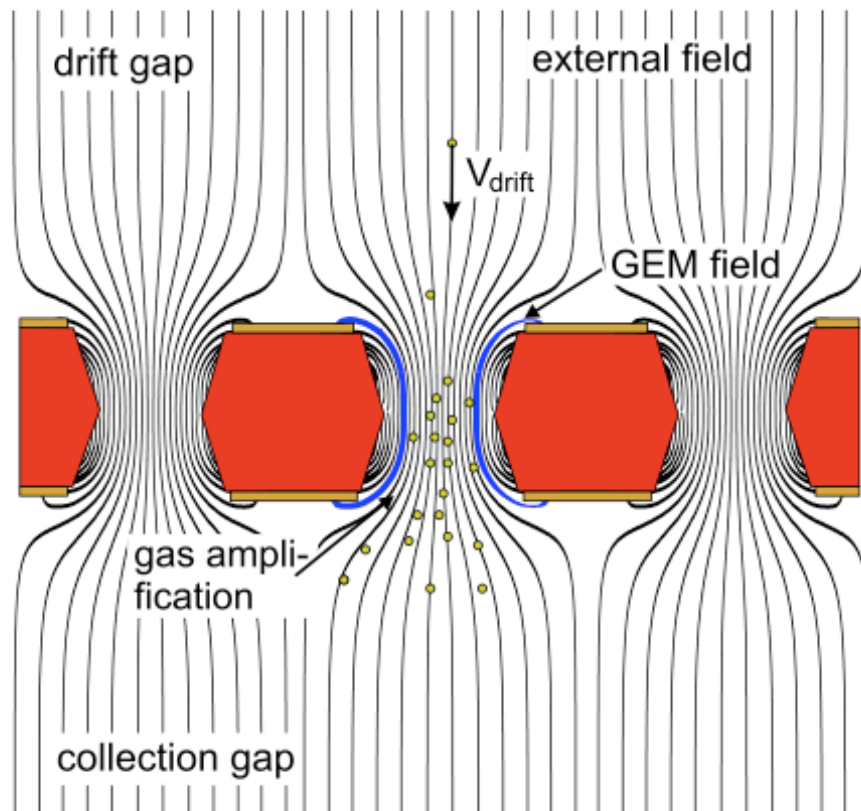


Thin, metal coated polyimide foil perforated with high density holes.

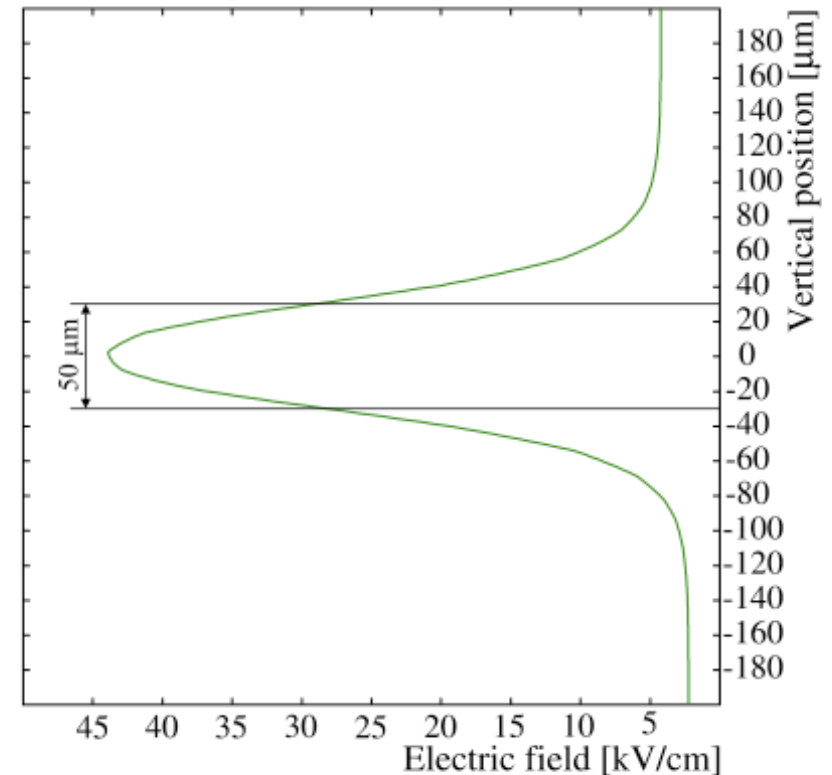


Electrons are collected on patterned readout board.
A fast signal can be detected on the lower GEM electrode for triggering or energy discrimination.
All readout electrodes are at ground potential.
Positive ions partially collected on the GEM electrodes.

GEM: Gas Electron Multiplier



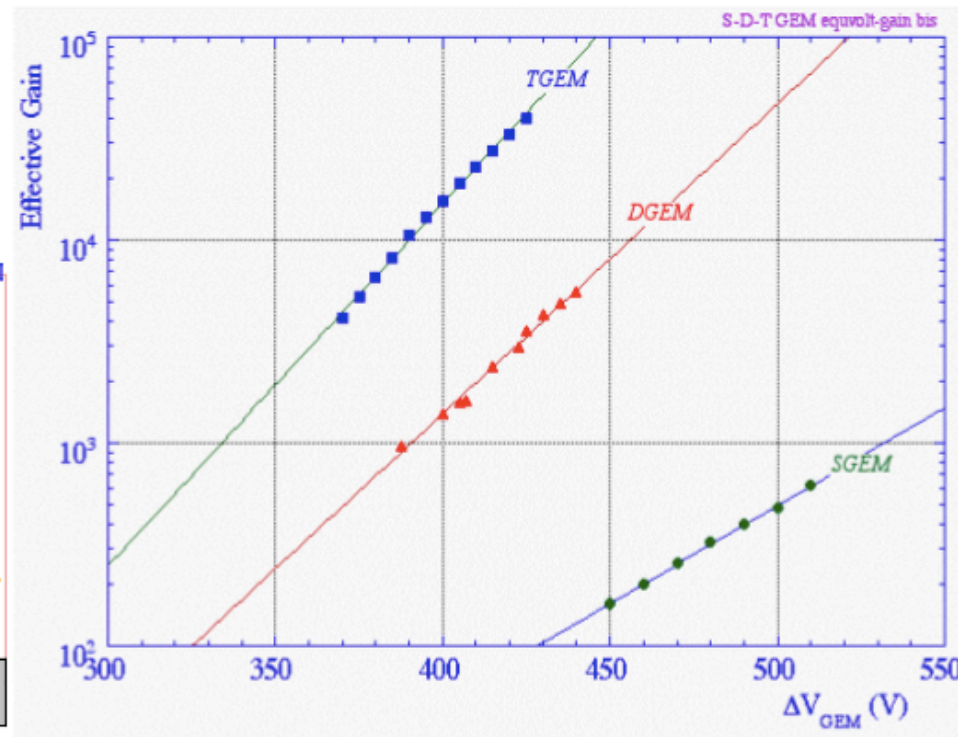
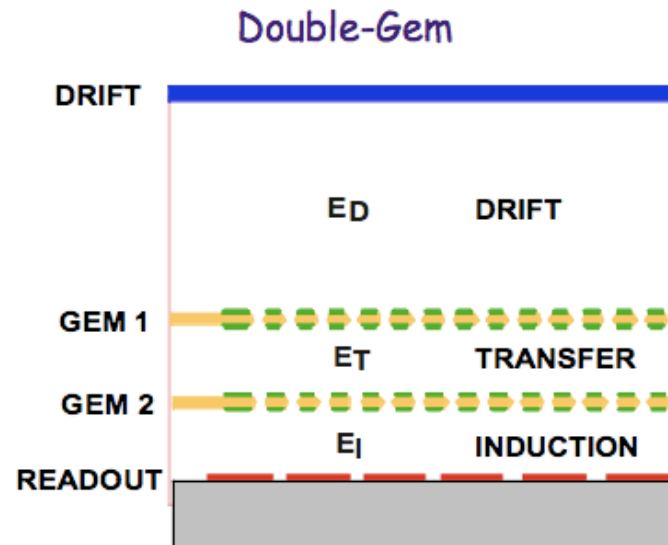
P. Cwetanski, thesis, Heidelberg



For a voltage between the GEM foils of 360 V the E-Field inside the gap reaches very high values, which cause gas amplification.

GEM Characteristics

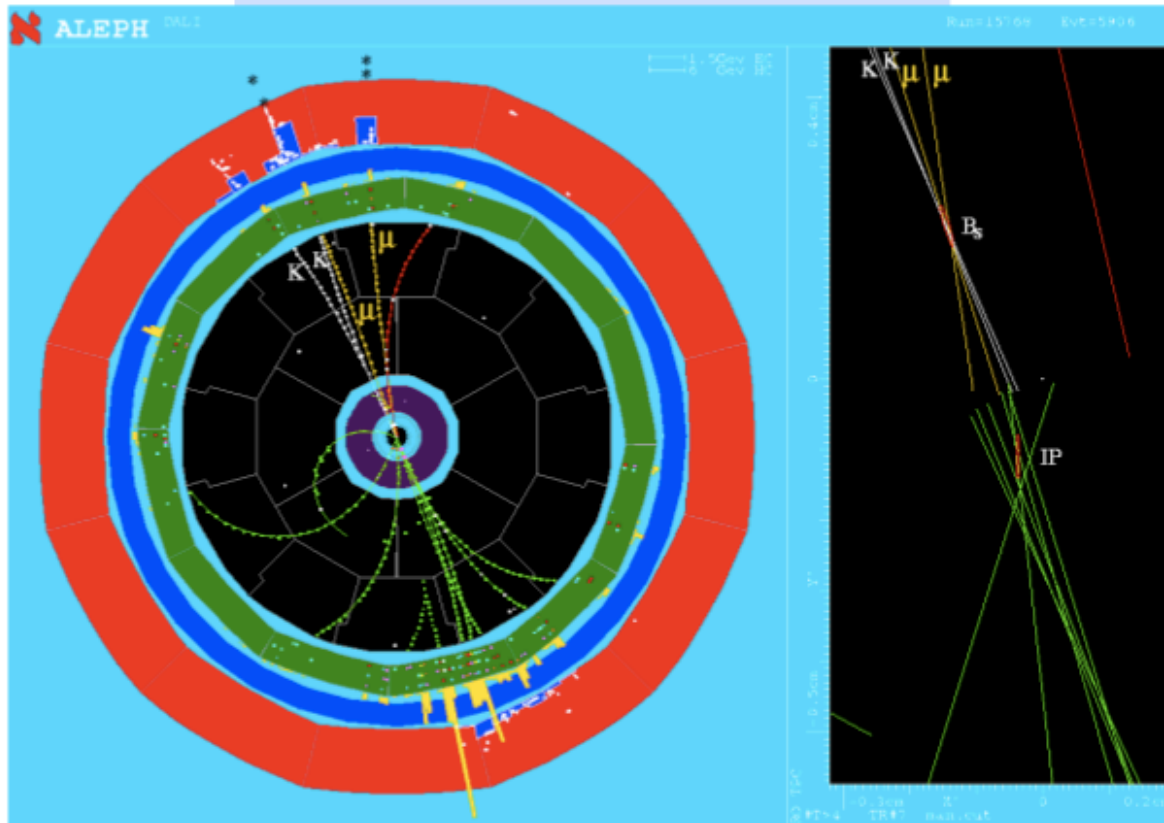
- Rate capability $\sim 1 \text{ MHz mm}^{-2}$
- Position accuracy (MIPs) $\sigma \sim 60 \mu\text{m}$
- Radiation tolerance $> 100 \text{ mC mm}^{-2}$
 - corresponds to $\sim 10^{14} \text{ MIPs cm}^{-2}$



Semiconductor Detectors

Need for semi-conductor tracker

$$B_s^0 \rightarrow \psi'(\rightarrow \mu^+ \mu^-) \phi(\rightarrow KK)$$

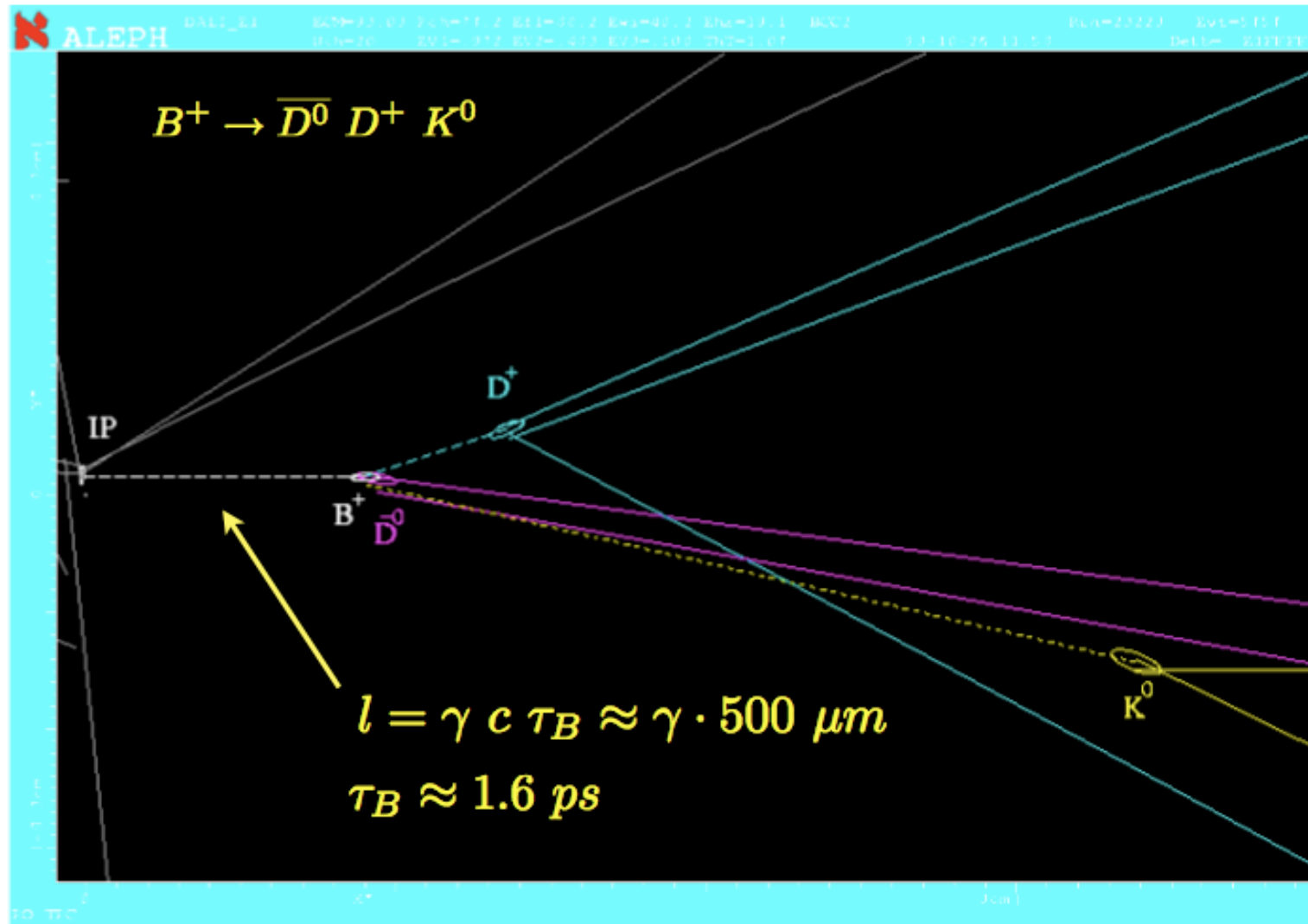


Aleph event:

Fully
reconstructed
 B_s decay.

Track measurements with a precision of a few μm near the interaction point improve the momentum measurement and allow to determine the decay vertex, especially important for bottom hadrons.

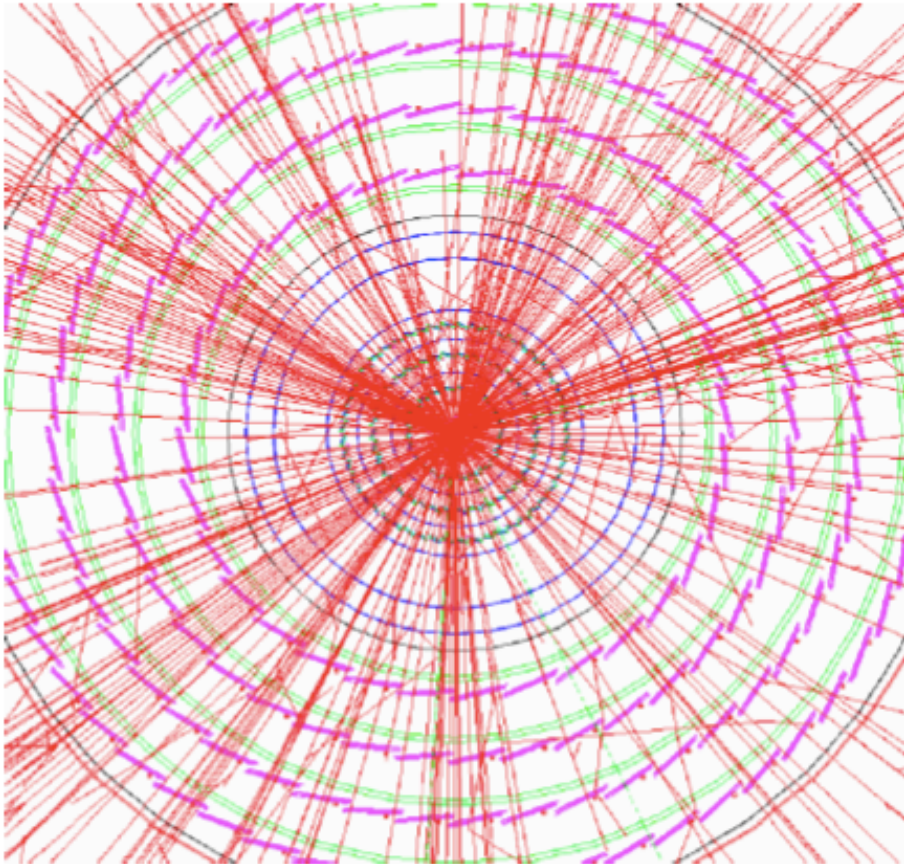
Vertex Reconstruction



The life time of B-mesons can be measured from the decay length l , if the momentum of the B-meson (γ -factor) is measured as well.

Vertexing at the LHC

$pp \rightarrow ttH$ ($m=120$ GeV)
 $H \rightarrow bb$
 $tt \rightarrow W(l\nu)b W(qq)b$



~ 1200 tracks/BX

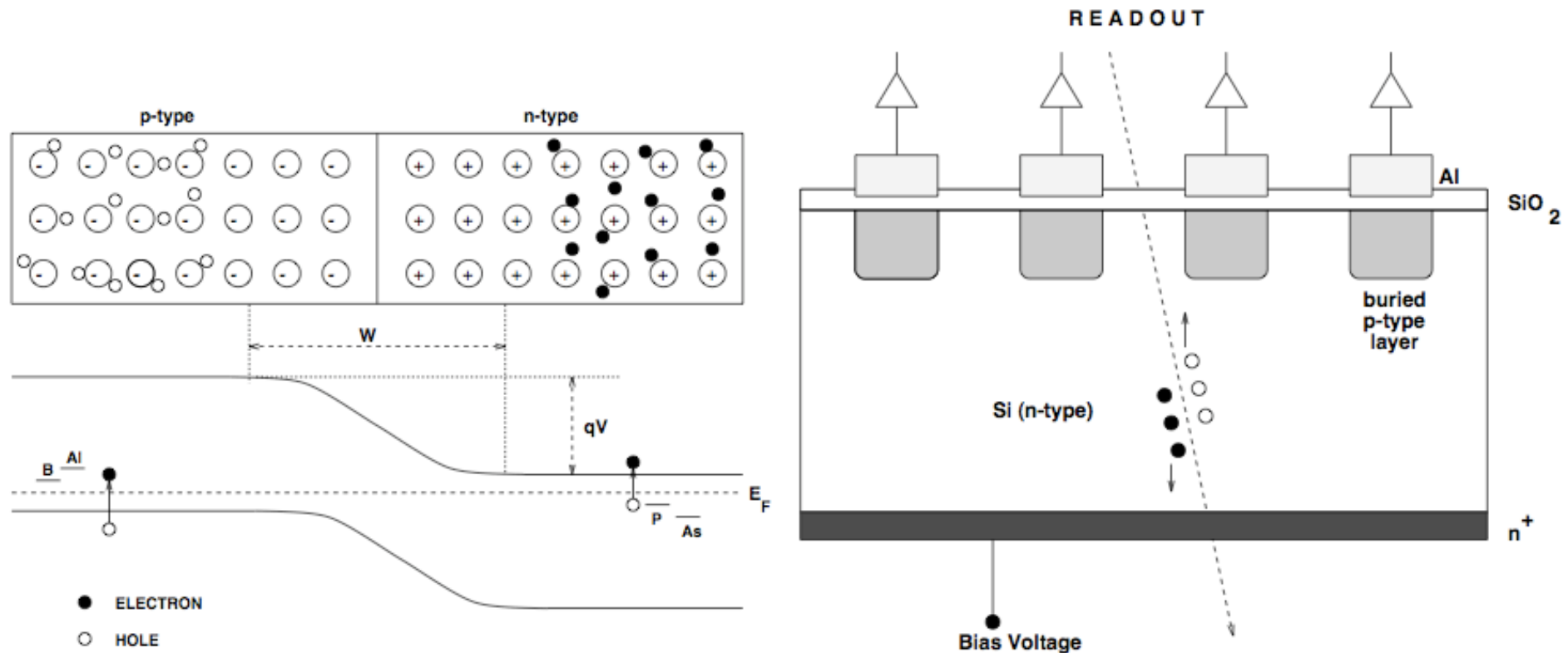
high track density
in particular in jets

3D hit information
mandatory



pixels

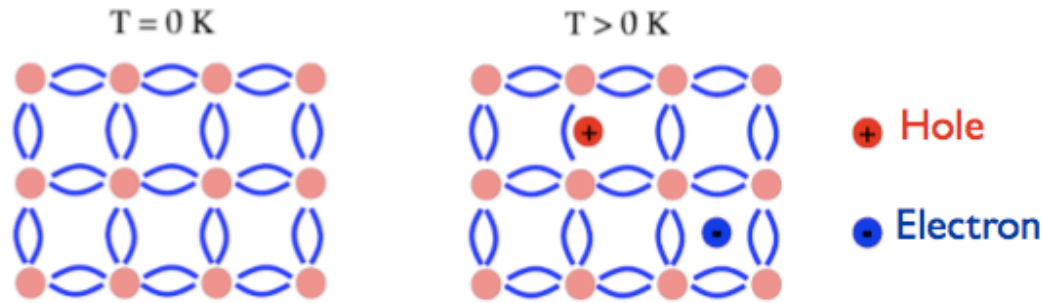
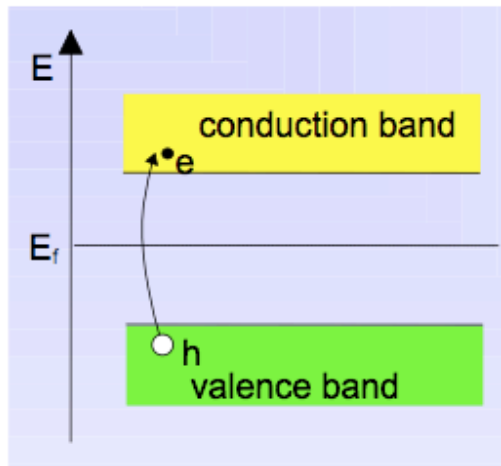
Solid State Tracking Detector - Silicon



p-n junction (diode).

Silicon:
 $dE/dx \approx 3.8 \text{ MeV/cm}$, Band Gap 1.1 eV
 3.6 eV to produce one electron-hole pair
 Typical thickness: 300 μm
 Strip Distance: $\geq 10 \mu\text{m}$

Doped Semiconductor Detectors



Silicon and germanium have 4 valence electrons, thus four covalent bounds. Thermal excitation excites electrons to the conduction band, which creates holes in the valence band.

Intrinsic electron(hole) concentration: $n_i = A T^{3/2} \exp(- E_g/2kT)$

(Si: Energy gap $E_g = 1.12 \text{ eV}$, Ge: $E_g=0.66 \text{ eV}$, $T=20 \text{ }^\circ\text{C} \Rightarrow kT=1/40 \text{ eV}$)

Typical values at $T = 300 \text{ K}$ (compare to silicon concentration of $5 \times 10^{22} \text{ cm}^{-3}$)

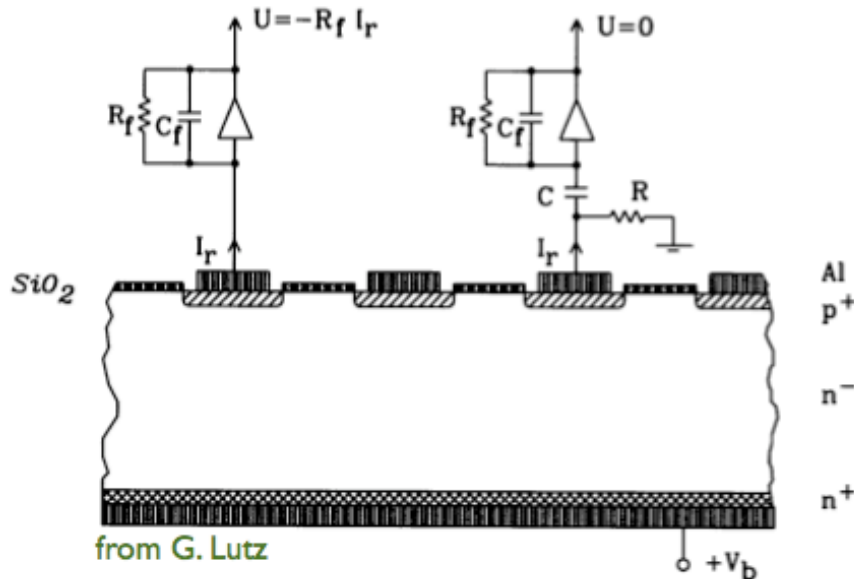
$$\text{Si: } n_i = 1.5 \times 10^{10} \text{ cm}^{-3}$$

$$\text{Ge: } n_i = 2.5 \times 10^{13} \text{ cm}^{-3}$$

Silicon Strip Detector

direct coupling

capacitive coupling



Direct coupling: reverse current I_r is absorbed by electronics.

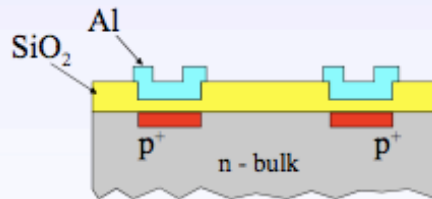
Capacitive coupling: AC part goes to amplifier, DC part goes through bias resistor R.

Typical detector thickness: 300 μm (150 μm - 500 μm)

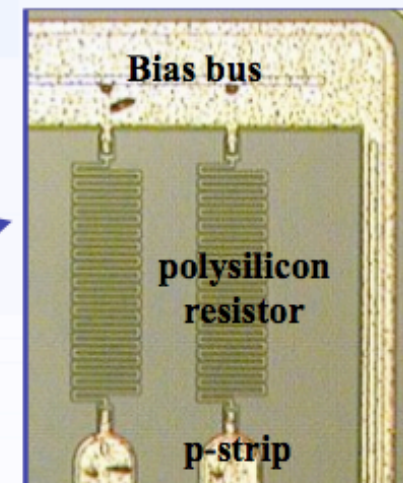
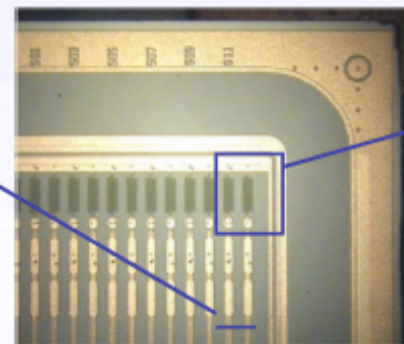
Typical strip separation, pitch p: 20 μm - 150 μm

Position resolution: $\sigma = p / \sqrt{12} = 14 \mu\text{m}$ ($p=50 \mu\text{m}$)

- Bias resistor produced by deposition of polysilicon.
- Capacitors produced via metal readout lines over implants (SiO_2 isolation).



Several different methods are used to readout strips and to provide bias voltage. They are implemented in the manufacturing process.



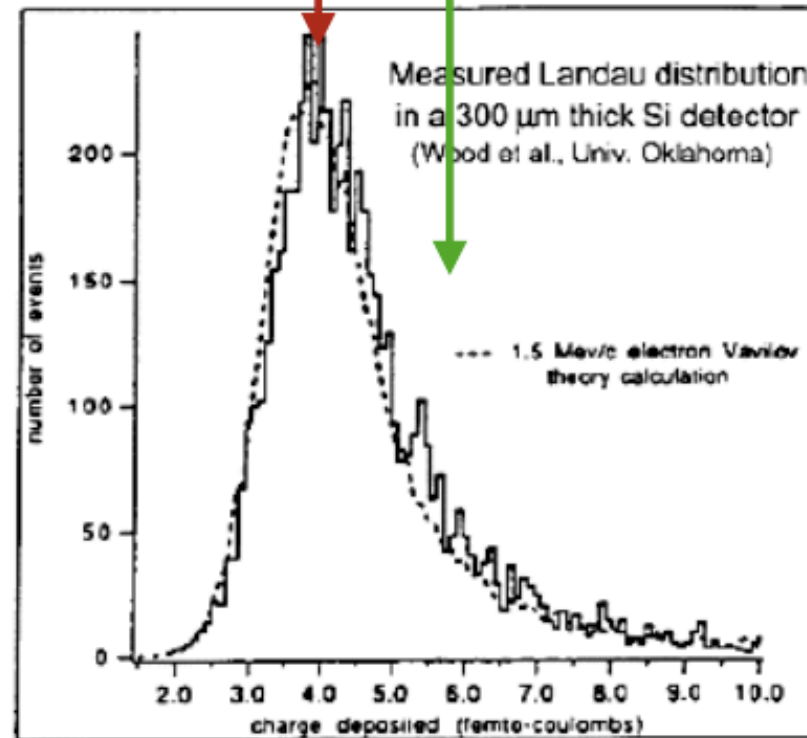
Measured Signal

Collected Charge for a Minimum Ionizing Particle (MIP)

- **Mean energy loss**
 dE/dx (Si) = 3.88 MeV/cm
⇒ 116 keV for 300 μ m thickness
- **Most probable energy loss**
 $\approx 0.7 \times$ mean
⇒ 81 keV
- **3.6 eV to create an e-h pair**
⇒ 72 e-h / μ m (mean)
⇒ 108 e-h / μ m (most probable)
- **Most probable charge (300 μ m)**
 ≈ 22500 e ≈ 3.6 fC

Most probable charge $\approx 0.7 \times$ mean

Mean charge



from M. Moll

Charge Collection and Diffusion

Charge collection time:

Drift velocity of charge carriers $v \approx \mu E$ and drift time $t_d = d/v = d/\mu E$.

Typical values: $d=300 \mu\text{m}$, $E=2.5 \text{ kV/cm}$ ($\mu_e=1350 \text{ cm}^2/\text{Vs}$ and $\mu_h=450 \text{ cm}^2/\text{Vs}$).

Drift times: $t_d(e) = 9 \text{ ns}$, $t_d(h) = 27 \text{ ns}$

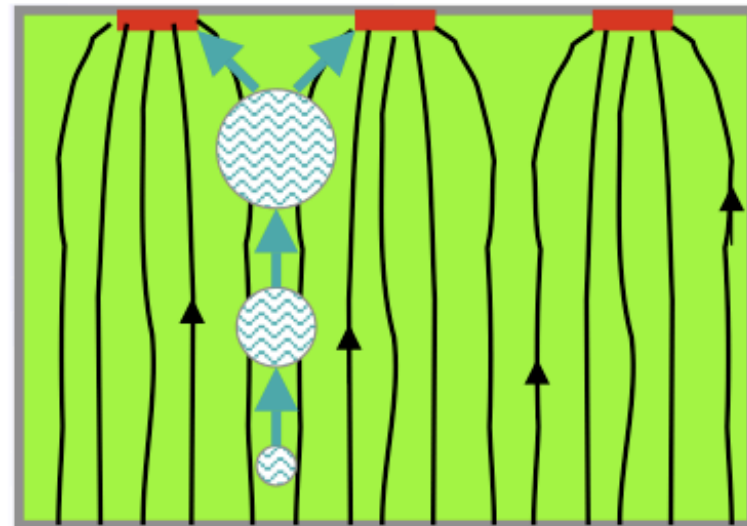
Diffusion:

Diffusion of charge cloud caused by scattering of charge carriers. Width of distribution increases with drift time t_d . Using the diffusion constant $D = \mu kT/e$ one finds:

$$\sigma = \sqrt{2Dt_d} = \sqrt{\frac{2dkT}{eE}}$$

Note that diffusion is the same for electrons and holes, since the mobility drops out.

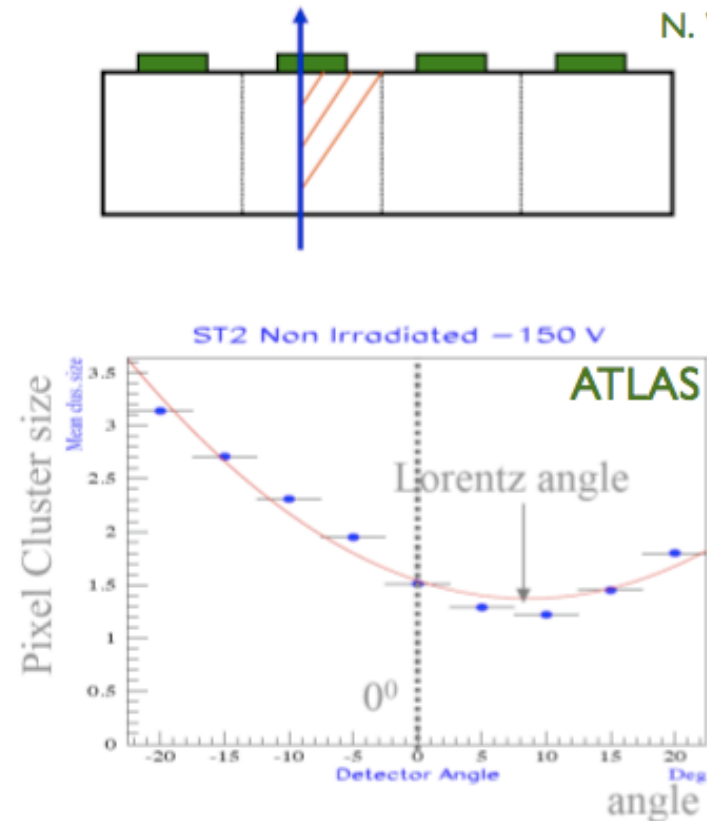
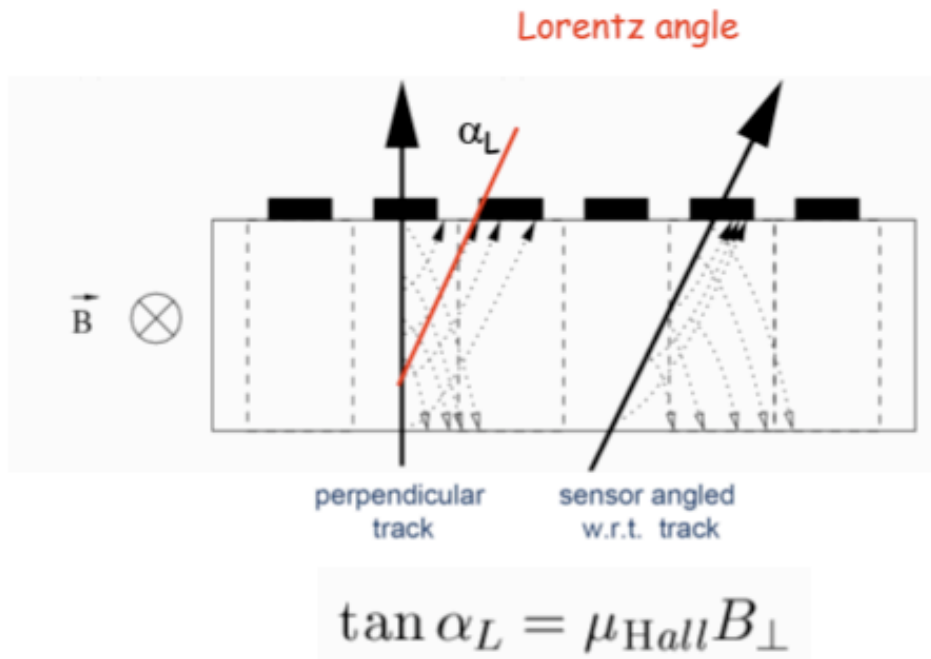
Typical charge width: 8-10 μm in 300 μm thick silicon. Width of charge cloud could be exploited to obtain better position resolution due to charge sharing between strips (**charge centroid finding**).



from M. Moll

Lorentz Angle in B-field

N. Wermes



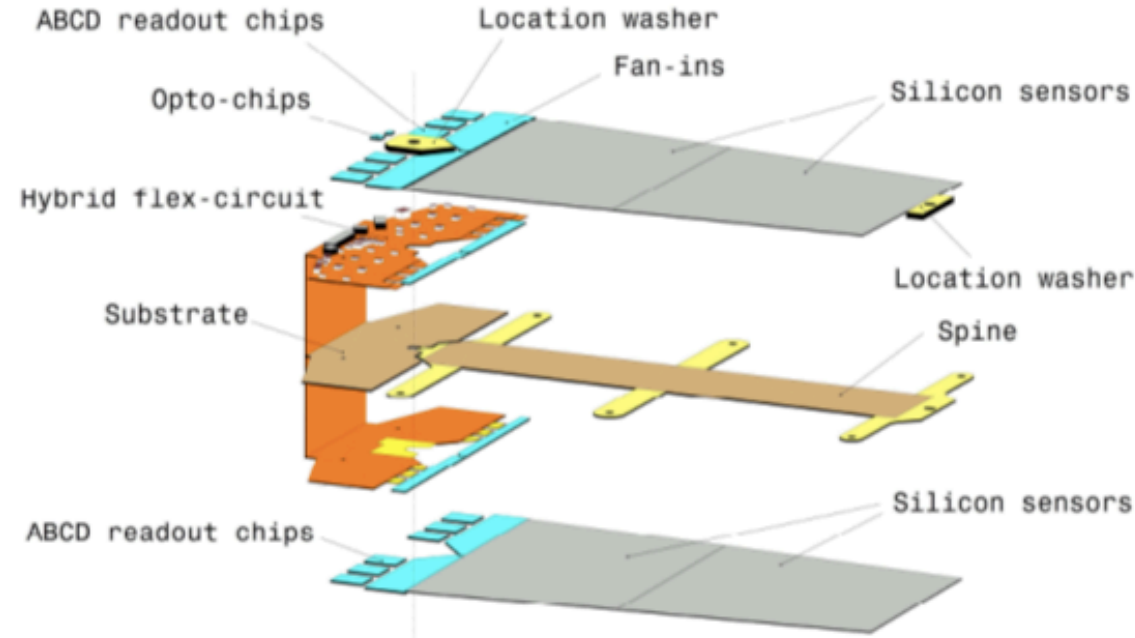
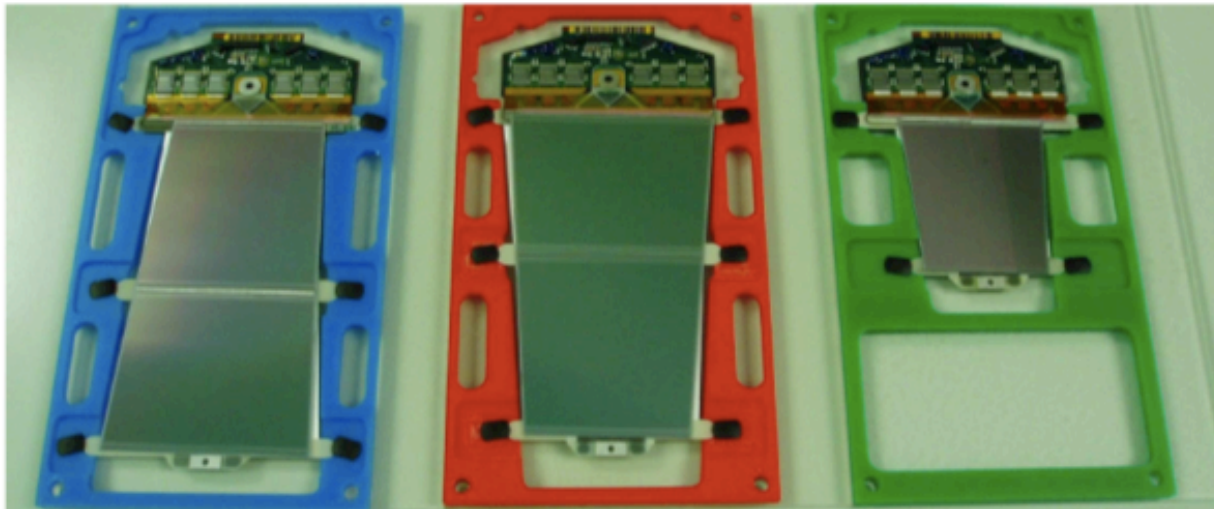
Measurement of Lorentz angle:

Number of strip (or pixel) hits is minimum, if incident angle of beam is equal to Lorentz angle.

Silicon detectors are built at a tilt angle to compensate for the Lorentz angle.

Effective incident angle = tilt angle + Lorentz angle

Detector Modules: ATLAS



ATLAS Silicon central tracker SCT

Endcap:

1976 modules with 2 sensors
glued back to back on spine.

Rotation by 20 mrad ($R\phi$ resolution)

Spine conducts heat.

Alignment position of sensors $\approx 2 \mu\text{m}$.

Strip pitch $80 \mu\text{m}$, width $12 \mu\text{m}$.

Resolution $16 \mu\text{m}$ in $R\phi$.

Operation temperature -7°C .

99.8% of strips are working.

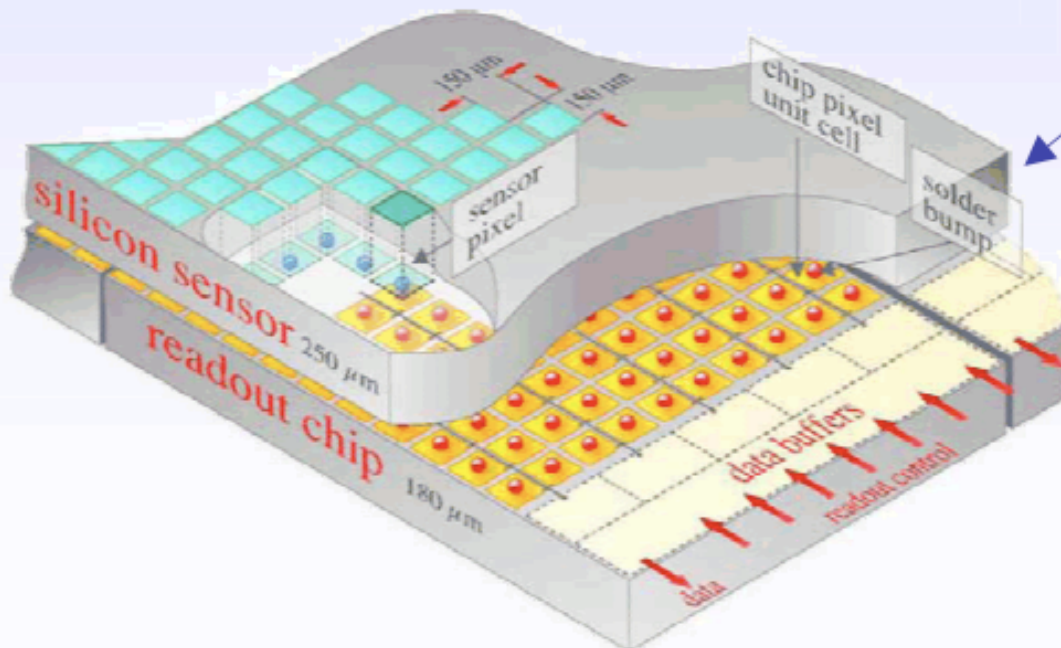
Other Silicon Detectors

- Double Sided Strip Detectors
 - Has strip structure also on back side, under 90°
 - Still no real 3d information
 - used to minimize material (multiple scattering)
 - more difficult to operate (noise)
- Silicon Drift
 - Same idea as (wire) drift chamber: Use time information
 - drift over several cm achieved (example: ALICE prototype)
- Silicon Pixel Detectors
 - No strips, but (usually rectangular) pixels
 - bonding for electronics very complicated, but doable (example: BTeV prototype)
 - give real 3d information
 - Usable for trigger

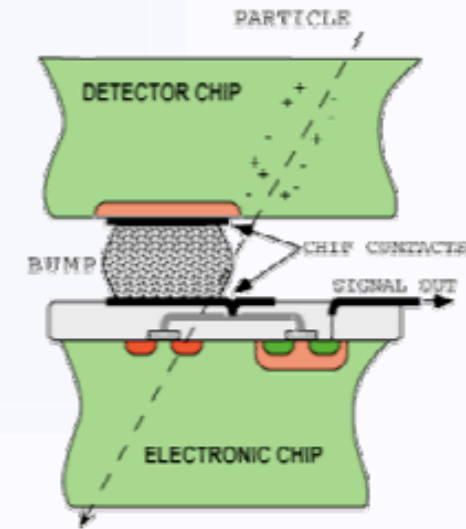
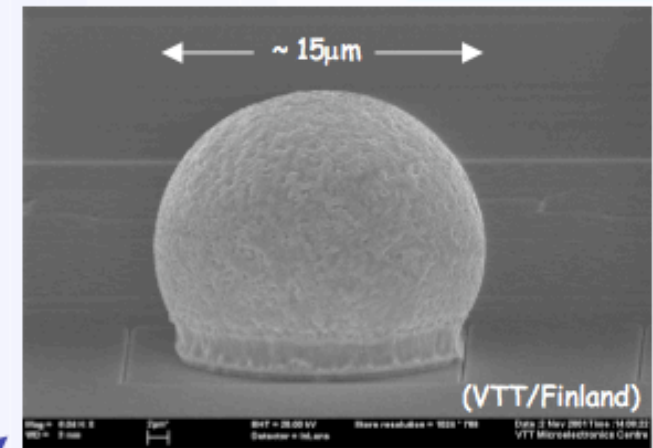
Hybrid Pixels

■ HAPS – Hybrid Active Pixel Sensors

- segment silicon to diode matrix with high granularity (⇒ true 2D, no reconstruction ambiguity)
- readout electronic with same geometry (every cell connected to its own processing electronics)
- connection by “bump bonding”
- requires sophisticated readout architecture
- Hybrid pixel detectors will be used in LHC experiments: ATLAS, ALICE, CMS and LHCb



Solder Bump: Pb-Sn

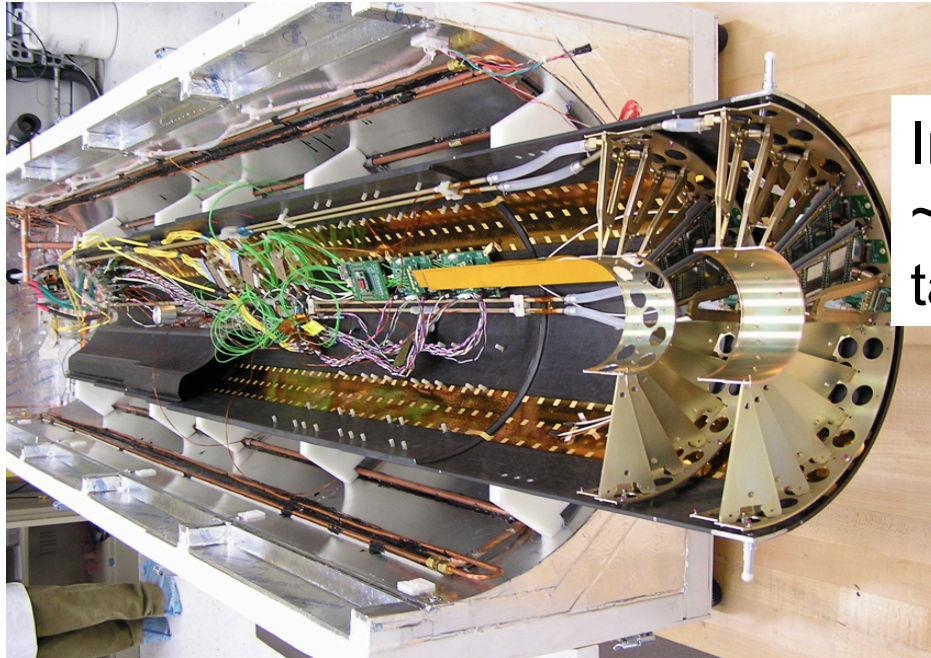


Flip-chip technique

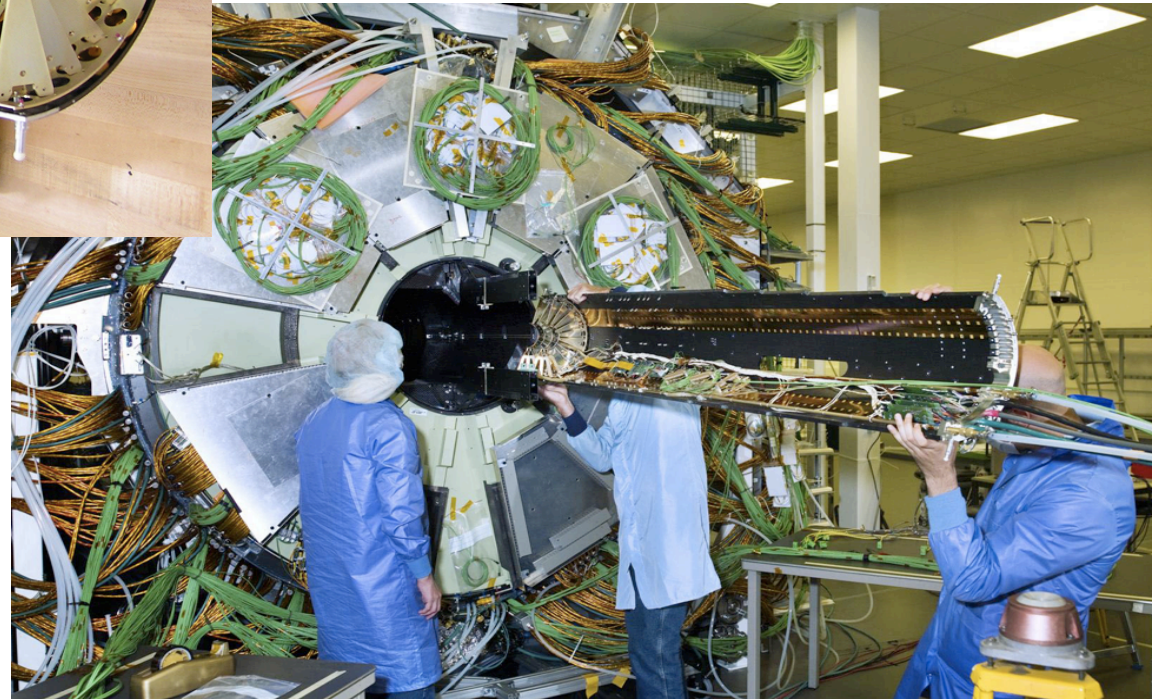


New Vertex Detector for CDF (or D0?). 1 Million strips

Pixel Tracking Detector



In total $7 \cdot 10^7$ read out channels
~ photo camera with 70 million pixels
taking 40 million photos per second!!

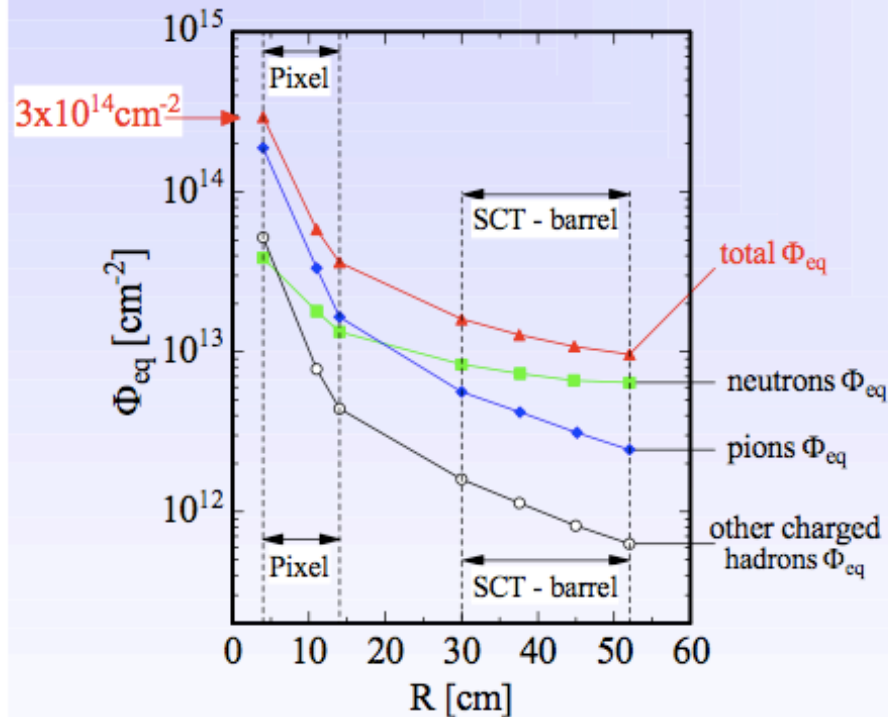


END

Radiation Damage

Example: ATLAS

- Fluences per year at full Luminosity



- Pixel detector: up to $\Phi_{eq} \approx 3.5 \cdot 10^{14} \text{ cm}^{-2}$ /year
- Dominating type of particle is different for pixel (pions) and strip detectors (neutrons)

LHC silicon detectors:

- All detectors have been extensively tested and developed for radiation tolerance and are expected to survive the LHC radiation environment.
- Some experiments have already foreseen upgrades (e.g. LHCb Velo after 3 years).

Super LHC

- upgrade of LHC to 10 x higher Luminosity
 - \Rightarrow 10 x higher radiation levels
 - \Rightarrow Radiation damage will become a critical issue!
- \Rightarrow New, radiation tolerant detectors needed!

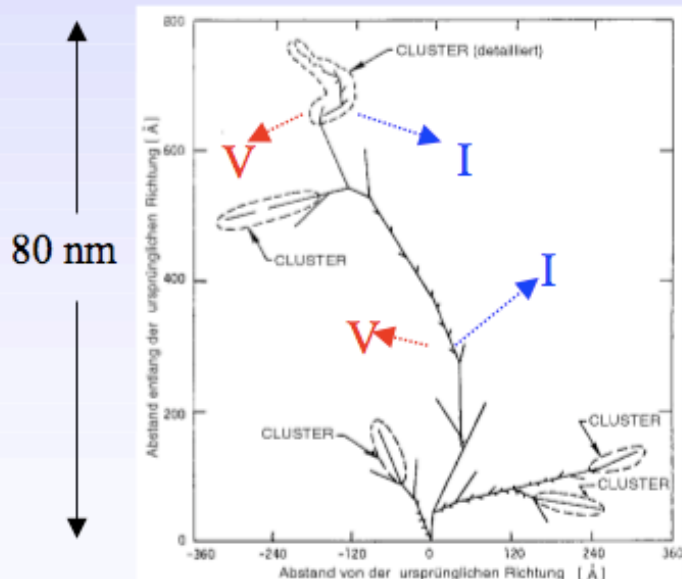
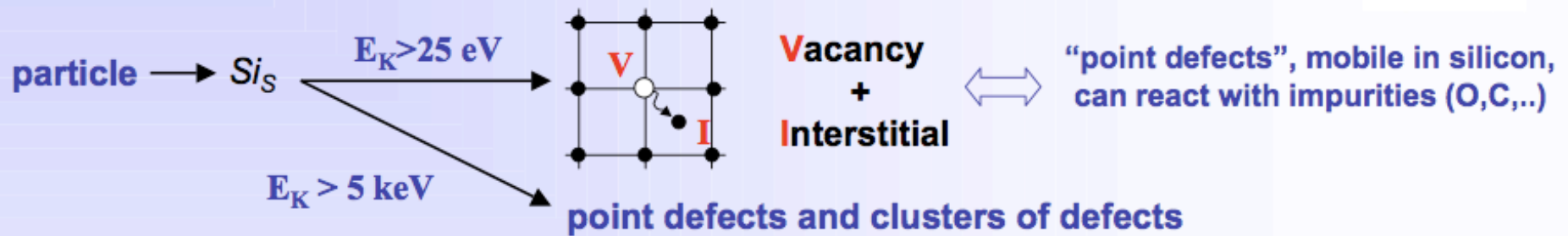
- What is radiation damage ?
- How to cope with it ?

from M. Moll

Radiation Damage

Damage to the silicon crystal: Displacement of lattice atoms

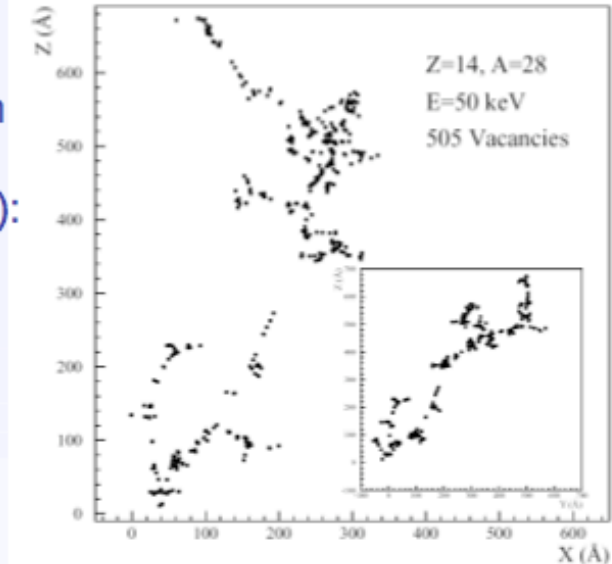
from M. Moll



Distribution of vacancies created by a 50 keV Si-ion in silicon (typical recoil energy for 1 MeV neutrons):

← Schematic [Van Lint 1980]

Simulation [M.Huhtinen 2001] →

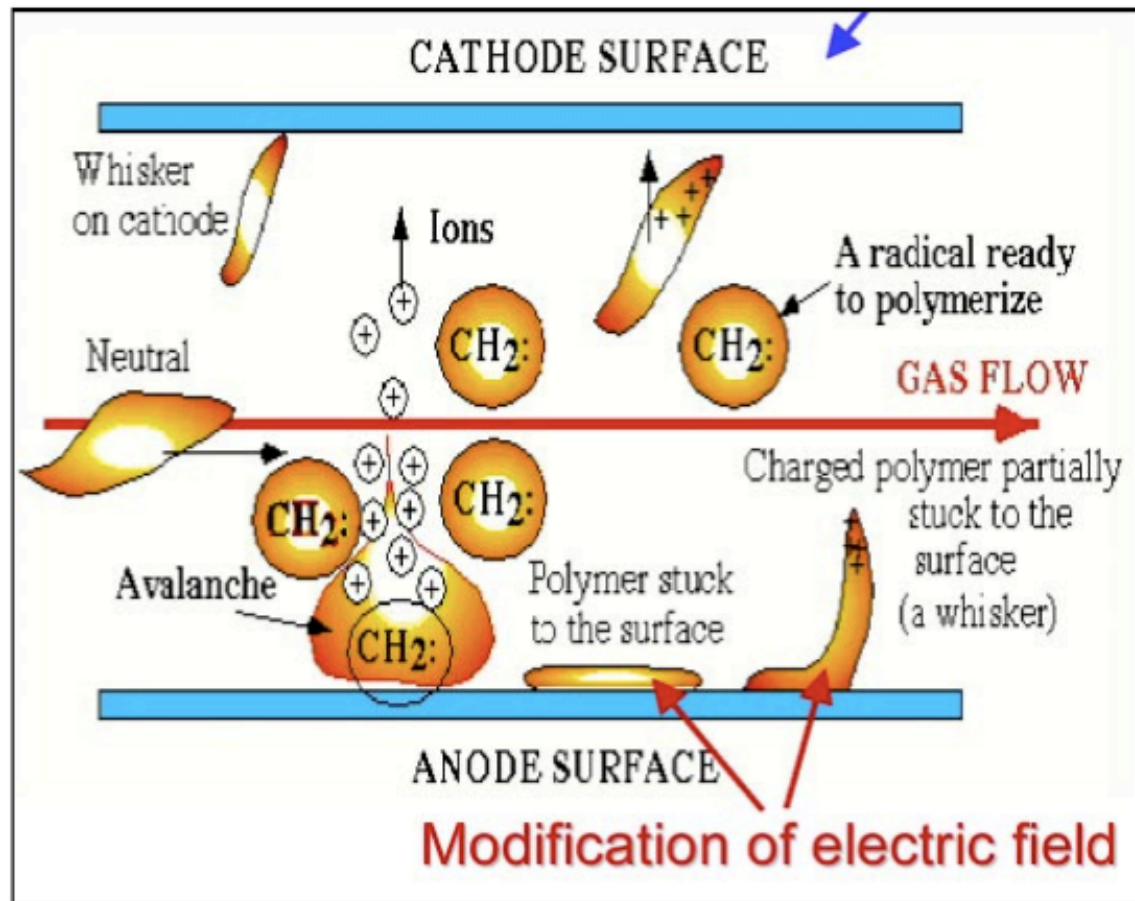


Defects can be electrically active (levels in the band gap)

- capture and release electrons and holes from conduction and valence band

\Rightarrow can be charged - can be generation/recombination centers - can be trapping centers

Detector Aging



Complex plasma-chemical reactions in the avalanche can lead to polymerization.

Deposits on anode and cathode.

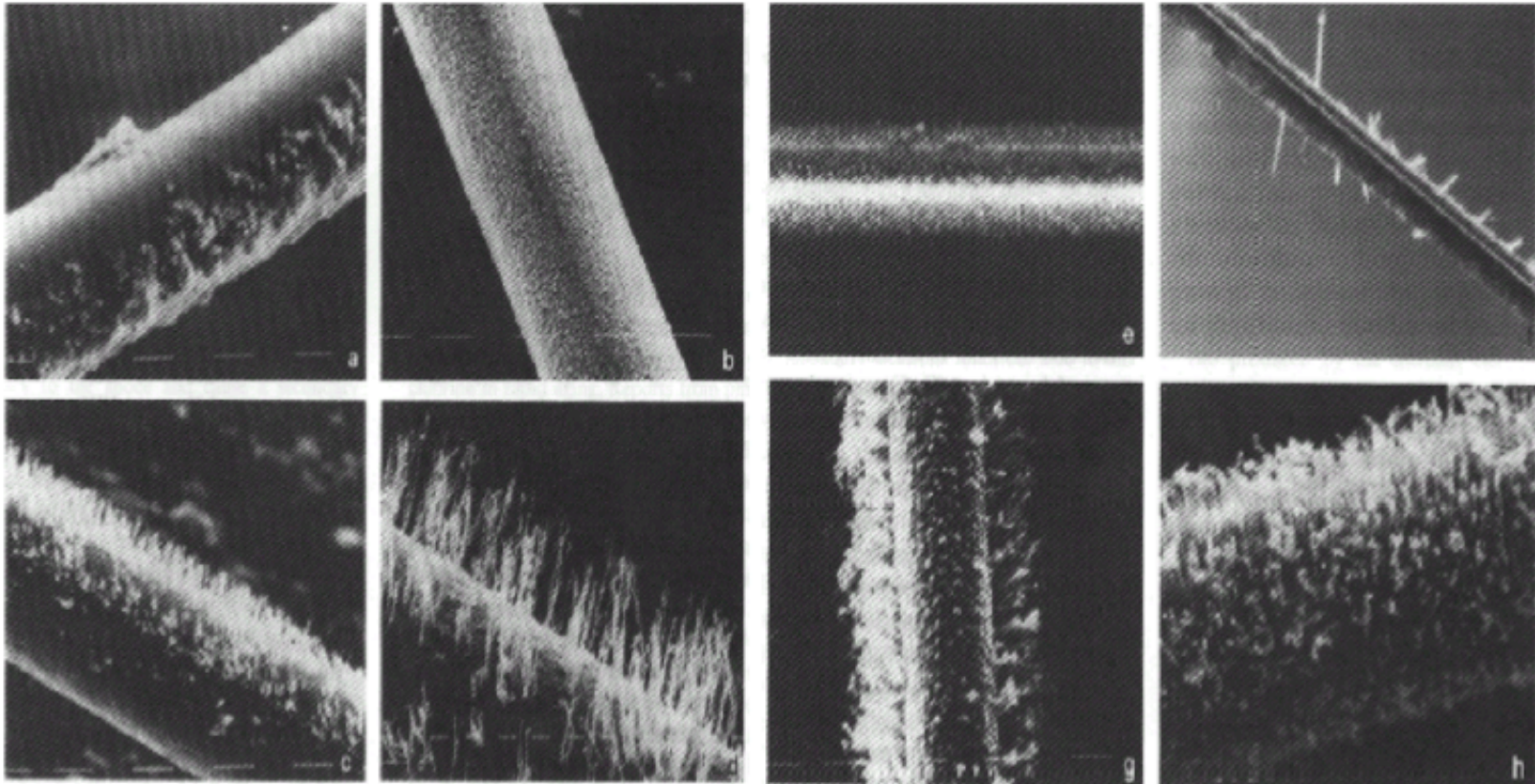
Deposits reduce electric field, which leads to reduced signal amplification (efficiency loss).

Malter effect:

Positive ions form a layer on cathode, high E-fields cause continuous electron extraction from cathode.

Leads to continuous discharge current.

Limitations of Gas Detectors



Whiskers are produced on the anode wire. They absorb the electrons. Thus electrons do not reach the main amplification region very close to the wire. This leads to **efficiency loss**.